ISTANBUL TECHNICAL UNIVERSITY ★ GRADUATE SCHOOL

VIBRATION CONTROL OF OFFSHORE STRUCTURES USING DEEP LEARNING PREDICTION METHODS

M.Sc. THESIS

Barış NAMLI

Department of Civil Engineering

Hydraulics and Water Resources Engineering Programme

JUNE 2022

ISTANBUL TECHNICAL UNIVERSITY ★ GRADUATE SCHOOL

VIBRATION CONTROL OF OFFSHORE STRUCTURES USING DEEP LEARNING PREDICTION METHODS

M.Sc. THESIS

Barış NAMLI
(501181520)

Department of Civil Engineering

Hydraulics and Water Resources Engineering Programme

Thesis Advisor: Assoc. Prof. Dr. Cihan BAYINDIR

JUNE 2022

İSTANBUL TEKNİK ÜNİVERSİTESİ ★ LİSANSÜSTÜ EĞİTİM ENSTİTÜSÜ

AÇIK DENİZ YAPILARININ TİTREŞİMLERİNİN DERİN ÖĞRENME ALGORİTMALARI İLE KONTROLÜ

YÜKSEK LİSANS TEZİ

Barış NAMLI
(501181520)

İnşaat Mühendisliği Anabilim Dalı

Hidrolik ve Su Kaynakları Mühendisliği Programı

Tez Danışmanı: Doç. Dr. Cihan BAYINDIR

HAZİRAN 2022

Barış NAMLI, a M.Sc. student of ITU Graduate School student ID 501181520 successfully defended the thesis entitled "VIBRATION CONTROL OF OFFSHORE STRUCTURES USING DEEP LEARNING PREDICTION METHODS", which he prepared after fulfilling the requirements specified in the associated legislations, before the jury whose signatures are below.

Thesis Advisor :	**Assoc. Prof. Dr. Cihan BAYINDIR** İstanbul Technical University & Boğaziçi University	.....
Jury Members :	**Prof. Dr. Mehmet ÖZGER** İstanbul Technical University	.....
	Assoc. Prof. Dr. Berna AYAT AYDOĞAN Yıldız Technical University	.....

Date of Submission : **10 May 2022**
Date of Defense : **03 June 2022**

To my family,

FOREWORD

I feel the happiness of completing my thesis due to work and effort during my master's period.
First of all, I would like to thank my advisor, Assoc. Prof. Dr. Cihan Bayındır for his support and help in writing my thesis. Without their help, this work would not have been possible. I would also like to thank him for sharing his knowledge and vision when we worked together.
I would like to thank my family, who supported me throughout the process. I am very lucky to have them.
I would like to thank my friends who showed their support to me at the point where I lost my motivation during the thesis process.
I would like to thank Prof. Dr. Mehmet Özger and Assoc. Prof. Dr. Berna Ayat Aydoğan for their contribution to improving my thesis.

June 2022

Barış NAMLI
Civil Engineer

TABLE OF CONTENTS

ABBREVIATIONS

AE	**:** Autoencoder
AMD	**:** Active Mass Damper
ANN	**:** Artificial Neural Network
CNN	**:** Convolution Neural Network
DBN	**:** Deep Belief Network
ER	**:** Electrorheological
FFT	**:** Fast Fourier Transform
FPS	**:** Floating Production System
FPSO	**:** Floating Production Storage Offloading
FSO	**:** Floating Storage Offloading
GA	**:** Genetic Algorithm
HMD	**:** Hybrid Mass Damper
LQR	**:** Linear Quadratic Regulator
LSTM	**:** Long Short Term Memory
MATLAB	**:** Matrix Laboratory
MF	**:** Magnification Factor
MLP	**:** Multilayer Perceptron
MR	**:** Magnetorheological
P-PVFM	**:** Physical Photovoltaic Forecasting Model
RBM	**:** Restricted Boltzmann Machine
RMSE	**:** Root Mean Square Error
RNN	**:** Recurrent Neural Network
TMD	**:** Tuned Mass Damper
TLCD	**:** Tuned Liquid Column Damper
TLD	**:** Tuned Liquid Damper
TLP	**:** Tension Leg Platform
VE	**:** Viscoelastic

SYMBOLS

a : Nodal Amplitude
A : Area
$\mathbf{A_s}$: Axial Area
B, **C** : Complex Amplitudes
b : Bias
c : Damping Coefficient
$\mathbf{c_c}$: Critical Damping
$\mathbf{C_D}$: Drag Coefficient
∇_h : Horizontal Gradient
$\mathbf{C_g}$: Group Velocity
$\mathbf{C_M}$: Lift Coefficient
D : Diameter
e : Error
E : Modulus of Elasticity
$\mathbf{E_\omega}$: Wave Energy
η : Water Surface Elevation
f : Frequency
f_c : Compressive Strength
F : External Force
$\mathbf{F_D}$: Control Force
$\mathbf{F_0}$: Amplitude of Force
$\mathbf{f_i}$: Forget Gate
ϕ : Velocity Potential
g : Gravitational Acceleration
G : Gyroscopic Matrix
$\mathbf{g_i}$: Input Gate
γ_{conc} : Unit Weight
h : Water Depth
$\mathbf{h_i}$: Hidden Layer
H : Wave Height
$\mathbf{H_D}$: Circulatory Matrix
$\mathbf{H_{1/3}}$: Significant Wave Height
k : Stiffness
$\mathbf{k_\omega}$: Wavenumber
$\mathbf{K_p}$, $\mathbf{K_v}$: Feedback Gain Matrices
L : Length of Structure
m : Mass
n : Ratio of Group Velocity

$\boldsymbol{\omega}$: Angular Frequency
$\mathbf{P_a}$: Atmospheric Pressure
$\boldsymbol{\rho}$: Density
$\mathbf{q}$: Displacement
$\mathbf{q_i}$: Output Gate
$\mathbf{S}$: Spectrum
$\mathbf{s_i}$: Cell State
$\boldsymbol{\sigma}$: Logistic Sigmoid Function
$\mathbf{S_k}$: Wavenumber Spectrum
$\mathbf{t}$: Time
$\mathbf{T}$: Period
$\mathbf{T_{1/3}}$: Significant Wave Period
$\boldsymbol{\theta}$: Symmetric Uniformly Distributed Random Phase
$\mathbf{u}$: Horizontal Velocity
$\mathbf{U}$: Input Weight
$\mathbf{V_{conc}}$: Volume of Concrete
$\mathbf{W}$: Recurrent Weight

LIST OF TABLES

Page

LIST OF FIGURES

Page

VIBRATION CONTROL OF OFFSHORE STRUCTURES USING DEEP LEARNING PREDICTION METHODS

SUMMARY

The structures have been built throughout history to meet many needs and contribute to the development of humanity. While some structures were built to accommodate people, some were built to fulfill people's work activities and allow activities in cultural, sports, and similar areas. Many activities can be done to develop humanity, thanks to the structures whose purpose of usage can change according to the region where they are built. The use of natural resources such as oil and natural gas has increased, especially in recent times in human history. In line with this development, natural resources were first extracted from the land. With the natural resources extracted from the land, the needs of the people have been met, and it has been seen that the living standards have increased over time. However, due to the increase in demand for natural resources over time, humanity needed to conduct research at points that it had not discovered before. In the early days, research was done at points close to the coast in line with the possibilities. Various structures were built in the regions where natural resources were found, and the resources obtained from there were started to be used. As time progresses, it has been determined that the opportunities have increased, and as a result, there are resources at deeper points than the coastal region, such as the ocean and sea. In order to obtain the resources identified in the open seas, structures called offshore structures were built. Examples of the increase in these opportunities are the development of technological, technical, and workforce development. Offshore structures can be defined under three subsections. These are fixed platforms, compliant platforms, and floating platforms. With the use of these structures, natural resources such as natural gas and oil obtained from the region where they are used are produced, stored, and offloaded according to the usage functions of the offshore platforms. In addition, drilling studies can be carried out to determine natural resources. In this way, it is seen that the natural resources necessary for human life and development can be provided sectorally.

Since offshore structures are important for their intended use, it is extremely critical to use the necessary technical information while designing and analyzing them. In addition, the structure must meet the conditions expected from it throughout its usage period. However, unlike the structures built on land, it is seen that the points to be considered while designing and constructing are different because they are exposed to different environmental conditions. Unlike structures on land, the wave is exposed to current force and glacial load. In addition, it is highly important to consider this factor when designing, since the previously mentioned harmonious and floating structures, unlike fixed structures, have a different connection with the ground in the region they are located. Under these conditions, it is observed that vibration occurs in the offshore structure. Earthquake load, dead load, wind load and the loads formed as a result of

the work done on the structure also affect the formation of vibration. Vibration in offshore structures prevents the structure from standing in balance. As a result of the deterioration of the balance, it becomes difficult for the structure to fulfill its usage function by displacement. Unlike the intended use, the safety and comfort of the people working in the structure may also be adversely affected due to the displacement that occurs as a result of vibration. Considering the studies in the literature in line with the reasons mentioned, it has been seen that various methods have been developed to control the vibration that occurs in offshore structures. Researches have shown that the vibration can be controlled by developing different systems according to the loading conditions. According to the results obtained, it has been seen that vibration control provides benefits both in terms of economy and safety. By controlling the vibration that occurs in the structure, possible damage will be prevented, and the usage function of the structure can be continued without any problems. In addition, it is seen that safety and working comfort are protected in line with the measures taken, and the approaches developed. Depending on the type of structure being built, the ways of achieving this balance are different. When the systems developed for vibration control are examined, it is seen that they are reliable, simple, and uncontrollable systems at the beginning. Over time, it has been observed that the control systems are more complex due to the developments in various fields, and the control capacity has increased. However, it has been seen from the studies that the developed control systems also have disadvantages.

One of the most recent developments has taken place in artificial intelligence. It is seen that artificial intelligence studies give better results than in the past, thanks to the storage of more data, the development of hardware that processes more, and the development of algorithms. Thanks to deep learning, which is one of the sub-branches of artificial intelligence that performs its operations by imitating the learning process of human beings, it is seen that successful results have been obtained in many areas. These areas are, for instance, computer vision, natural language processing, customer relationship management. In addition, it has been seen that it gives effective results in time series forecasting. Thanks to the studies carried out in time series analysis, it is possible to forecast the future by using the information belonging to the previous times and the current time. In this way, it is seen that successful results have been achieved in finance, economy, and planning. Thanks to the ability to forecast for the future can benefit the planning and organization of the current situation. Time-series forecasting using deep learning can be done in hydraulics and coastal engineering as well as in finance, economics, planning. In coastal engineering, forecasting external forces that may affect offshore structures can be extremely useful for coastal planning.

This study it is aimed to reduce offshore platform's vibration parameters the displacement caused by forecasting the wave forces affecting the offshore structure using a deep learning algorithm and giving feedback to the system. For this purpose, the numerical solution to be applied is compared with the analytical solution as a benchmark problem. Then, the monochromatic Morison wave force acting on the theoretically constructed system was calculated using the Morison equation. The calculated wave force was forecasted using the long short term memory (LSTM)

algorithm. The forecasted wave force is given as feedback to the system. In the last study, the wave field was created using the wave spectrum to evaluate the system realistically. Theoretically, the multichromatic Morison wave force acting on the Draugen platform placed in the middle of the wave field was forecasted using the LSTM algorithm. The forecasted multichromatic Morison wave force is applied to the system as feedback. The obtained results are discussed over whether the vibration control can be performed successfully or not.

AÇIK DENİZ YAPILARININ TİTREŞİMLERİNİN DERİN ÖĞRENME ALGORİTMALARI İLE KONTROLÜ

ÖZET

Yapılar tarih boyunca pek çok ihtiyacı karşılamak ve insanlığın gelişimine katkı sağlamak için inşa edilmişlerdir. Bazı yapılar insanların barınabilmesi için inşa edilmişken bazıları insanların çalışma faaliyetlerini yerine getirmek, kültürel, spor ve benzeri alanlarda çalışmaların yapılmasına olanak sağlamak için inşa edilmiştir. Kullanım amacı da inşa edildiği bölgeye göre değişebilen yapılar sayesinde insanlığın gelişimi için pek çok faaliyet yapılabilmektedir. İnsanlık tarihinin özellikle son zamanlarında petrol ve doğalgaz gibi doğal kaynakların kullanımı artmaktadır. Bu gelişim doğrultusunda kullanılan doğal kaynaklar ilk olarak karadan çıkarılmaya başlanmıştır. Karadan çıkarılan doğal kaynaklar sayesinde insanların ihtiyaçları karşılanmış ve yaşam standartlarının zamanla arttığı görülmüştür. Ancak zaman içerisinde doğal kaynaklara karşı talebin artması sonucunda insanlık daha önceden keşfetmediği noktalarda da araştırmalar yapmaya ihtiyaç duymuştur. İlk zamanlarda eldeki imkanlar doğrultusunda kıyıya yakın noktalarda araştırmalar yapılmış doğal kaynakların bulunduğu bölgelere çeşitli yapılar inşa edilmiş ve buradan elde edilen kaynaklar kullanılmaya başlanmıştır. Zaman ilerledikçe çeşitli alanlarda yaşanan gelişmelerin artmasıyla beraber imkanların arttığı, bunun sonucunda okyanus ve deniz gibi kıyı bölgesinden daha derin noktalarda da kaynakların bulunduğu tespit edilmiştir. Açık denizlerde tespit edilen kaynakların elde edilebilmesi için açık deniz yapıları adı verilen yapılar açık denizlerde inşa edilmiştir. Bu imkanların artmasına teknolojik gelişmelerin oluşması, çeşitli alanlar üzerinde yapılan çalışmalar sonucunda teknik bilginin geliştirilmesi ve uygulanacak olan iş gücünün gelişmesi örnek verilebilir. Açık deniz yapıları üç alt bölüm altında tanımlanabilir. Bunlar sırasıyla sabit platformlar, uyumlu platformlar ve yüzen platformlardır. Bu yapıların kullanılmasıyla birlikte kullanıldığı bölgeden elde edilen doğalgaz, petrol gibi doğal kaynakların, açık deniz yapılarının kullanım fonksiyonlarına göre üretildiği, elde edildiği, depolandığı ve aktarıldığı görülmektedir. Ayrıca doğal kaynakların tespiti için sondaj çalışmaları da yapılabilmektedir. Bu sayede sektörel olarak, insan yaşamı ve gelişimi için gerekli olan doğal kaynakların temin edilebildiği görülmektedir.
Açık deniz yapıları kullanım amacına göre son derece önemli yapılar olduğu için gerekli olan teknik bilginin dizayn ve analiz edilirken kullanılması son derece kritiktir. Ayrıca yapının kullanım süresi boyunca kendisinden beklenen şartları sağlaması gerekmektedir. Ancak karada inşa edilen yapılardan farklı olarak farklı çevre koşullarına maruz kaldığı için tasarlanırken ve inşa edilirken dikkat edilmesi gereken noktaların farklı olduğu görülmektedir. Karadaki yapılardan farklı olarak dalga, akıntı kuvvetine ve buzul yüküne maruz kalmaktadır. Ayrıca daha önce söz edilen uyumlu ve yüzen yapıların sabit yapıların aksine bulunduğu bölgede zeminle olan bağlantısı

farklı olduğu için dizayn edilirken bu faktörün de göz önünde bulundurulması son derece önemlidir. Bu şartlar altında açık deniz yapısında titreşimin oluştuğu görülmektedir. Ayrıca deprem yükü, ölü yük, rüzgar yükü ve yapıda yapılan çalışmalar sonucunda oluşan yüklerin de titreşim oluşmasına etkisi olmaktadır. Açık deniz yapılarında oluşan titreşim yapının dengede durmasını engeller. Dengenin bozulması sonucunda yer değiştirme yaparak yapının kullanım fonksiyonun yerine getirmesi zorlaşmaktadır. Kullanım amacından farklı olarak titreşimin olması sonucunda oluşan yer değiştirme nedeniyle yapıda çalışan insanların güvenliği ve konforu da olumsuz etkilenebilmektedir. Bahsedilen nedenler doğrultusunda literatürde yapılan çalışmalara bakıldığında açık deniz yapılarında oluşan titreşimi kontrol altına alabilmek için çeşitli yöntemlerin geliştirildiği görülmüştür. Yapılan araştırmalar yükleme durumlarına göre farklı sistemler geliştirerek oluşan titreşimin kontrol altına alınabildiğini göstermiştir. Elde edilen sonuçlara göre titreşim kontrolünün hem ekonomik hem de güvenlik açısından fayda sağladığı görülmüştür. Ekonomik olarak yapıda oluşan titreşimin kontrol edilmesiyle birlikte hasar oluşumu engellenecek ve yapının kullanım fonksiyonuna sorunsuz bir şekilde devam edilebilecektir. Ayrıca can güvenliğinin ve çalışma konforunun alınan önlemler ve geliştirilen yaklaşımlar doğrultusunda korunduğu görülmektedir. İnşa edilen yapının türüne göre bu dengeyi sağlama şekilleri farklıdır. Titreşim kontrolü için geliştirilen sistemlere bakıldığında başlangıçta güvenilir, basit ve kontrol edilemeyen sistemler olduğu görülmektedir. Zamanla çeşitli alanlarda yaşanan gelişmeler nedeniyle kontrol sistemlerinin daha karmaşık olduğu ancak kontrol kapasitesinin arttığı gözlemlenmiştir. Yine de geliştirilen kontrol sistemlerinin de sahip olduğu dezavantajların olduğu yapılan çalışmalar sonucunda görülmüştür.

Son zamanlarda yaşanan gelişmelerden biri de yapay zeka alanında gerçekleştirilmiştir. Çalışmalar neticesinde daha fazla verinin depolanabilmesi, teknolojik olarak daha fazla işlem yapabilen donanımların geliştirilmesi ve algoritmaların geliştirilmesi sayesinde geçmişe göre yapay zeka çalışmalarının daha iyi sonuç verdiği görülebilmektedir. İnsanın öğrenme sürecini taklit ederek işlemlerini gerçekleştiren yapay zekanın alt dallarından biri olan derin öğrenme sayesinde pek çok alanda başarılı sonuçlar elde edildiği görülmektedir. Bu alanlardan bazıları bilgisayar görüsü, doğal dil işleme, müşteri ilişkileri yönetimidir. Ayrıca zaman serisi tahmininde de etkili sonuçlar verdiği görülmüştür. Zaman serisi analizi alanında yapılan çalışmalar sayesinde daha önceki zamanlarda ve mevcut zamana ait olan bilgiler kullanılarak geleceğe yönelik tahmin yapılabilmektedir. Bu sayede finans, ekonomi, planlama alanlarında başarılı sonuçların elde edildiği görülmektedir. Geleceğe yönelik tahminlerin yapılabilmesi sayesinde mevcut durumun planlanmasında ve organize edilmesine fayda sağlayabilmektedir. Derin öğrenme kullanılarak yapılan zaman serisi tahmini finans, ekonomi, planlama alanlarında olduğu gibi hidrolik ve kıyı mühendisliğinde de yapılabilmektedir. Kıyı mühendisliği alanında açık deniz yapılarına etki edebilecek olan dış kuvvetlerin tahmin edilmesi kıyı planlaması için son derece faydalı olabilir.

Bu çalışmamızda açık deniz yapısına etki eden dalga kuvvetleri derin öğrenme algoritması kullanılarak tahmin edilip sisteme geri besleme olarak verilerek oluşan

yer değiştirmenin azaltılması amaçlanmıştır. Bunun için öncelikle uygulanacak olan hesaplamalı çözüm yöntemi analitik çözüm yöntemiyle karşılaştırılmıştır. Daha sonra teorik olarak oluşturulmuş sisteme etki eden tek zamanlı Morison dalga kuvveti Morison denklemi kullanılarak hesaplanmıştır. Hesaplanan dalga kuvveti LSTM algoritması kullanılarak tahmin edilmiştir. Tahmin edilen dalga kuvveti sisteme geri besleme olarak verilmiştir. En son çalışmada ise sistemin gerçekçi bir şekilde değerlendirilebilmesi için dalga spektrumu kullanılarak dalga sahası oluşturulmuştur. Dalga sahasının tam ortasına teorik olarak yerleştirilmiş tek ayaklı betonarme yapıya etki eden çok zamanlı Morison dalga kuvveti derin öğrenme algoritmalarından biri olan LSTM algoritması kullanılarak tahmin edilmiştir. Tahmin edilen çok zamanlı Morison dalga kuvveti sisteme geri besleme olarak uygulanmaştır. Elde edilen sonuçlar titreşim kontrolünün başarılı bir şekilde gerçekleştirilip gerçekleştirilemediği üzerinden tartışılmıştır.

1. INTRODUCTION

Vibration is one of the concepts that should be considered in civil engineering, which can occur continuously or momentarily as a result of the dynamic feature of the world. It should be taken into account that negative effects on sectoral, economic, and human life may occur if the vibration in the structures is not taken into consideration. Vibration is the periodic motion of an object leaving its equilibrium position [1]. It is vital to consider the external factors that may cause the structure to displace from its equilibrium position and the properties of the structure. These structures cannot maintain their equilibrium positions and start to vibrate because of external factors such as wave motion, tides, and earthquake load. Consequently, the work on the structure can be prevented. Also, the safety and comfort of the people working in the structure are adversely affected. Many studies have been carried out in the literature to control vibration in offshore structures. In the control studies carried out taking into account the characteristics of external factors, it is seen that control is made according to many factors such as regular and irregular wave load, tidal current, and earthquake load, as mentioned before. In this thesis, vibration control is carried out with a deep learning algorithm, which is one of the artificial intelligence methods that is frequently used today, unlike the studies in the literature.

1.1 Purpose of Thesis

In marine engineering, it is seen that the vibration that occurs in offshore structures has a serious effect. There may be negative economic effects such as damage to the structure and prevention of work in the structure. In addition, the life safety and comfort of the people working in the structure are adversely affected, apart from its economic aspect. In order to prevent the occurrence of such damages, various studies have been carried out in the literature to control and reduce the vibration that occurs in offshore structures. Especially since waves are one of the most complex

and variable factors in nature, there are studies in which wave motions are taken into account as realistically as possible, and their effects are represented and evaluated [2]. When we look at the studies, simple and uncontrollable systems are used according to technological possibilities. However, some studies use more intelligent systems that can be controlled over time. It is believed that progress can be made in vibration control according to the developments in many fields, especially with the artificial intelligence studies that have an importance in recent times.

The main purpose of this study is to control the multichromatic Morison wave forces affecting the single-legged reinforced concrete offshore structure built in the wave field created by using the wavenumber spectrum together with LSTM, which is one of the sub-branches of artificial intelligence and to control the displacement. Another aim is to control the structure's vibration by controlling the monochromatic Morison waves.

In the continuation of Chapter 1, studies on vibration control and time series forecasting in the literature are mentioned.

In Chapter 2, offshore structures that are frequently used were explained. The usage areas, features, advantages, and disadvantages of offshore structures are explained.

In Chapter 3, vibration control systems were explained. The features, advantages, and disadvantages of the systems were mentioned. Afterward, vibration controls in offshore structures were discussed. Three different studies conducted in the thesis are explained in this section. The first study is to compare the analytical solution with the numerical solution and evaluate the numerical solution results both in the time domain and in the frequency domain. The second study is vibration control of the structure under monochromatic Morison wave load by using the LSTM algorithm. In the third study, the vibration is controlled using the LSTM algorithm on the structure under multichromatic Morison wave load. The calculations required to carry out these studies are explained in detail.

In chapter 4, information about deep learning is given. The role of deep learning in time series forecast and the common deep learning algorithms are explained, and the LSTM algorithm used for the study is explained. Finally, vibration controls using deep learning are explained.

In Chapter 5, the results of three different studies are explained and discussed. In the first study, the analytical and numerical solutions were compared, and the accuracy of the numerical solution was verified. The second study shows the results of vibration control using the LSTM algorithm against monochromatic Morison force affecting the structure. In the third study, the effects of multichromatic Morison wave force on the Draugen platform placed in the middle of a realistic wave field and the vibration control study using LSTM are explained. The results were analyzed in the time domain and frequency domain.

In Chapter 6, the results obtained in the study were evaluated. Recommendations that can be used for future work are indicated.
Contributing to the literature and guiding researchers who will work on these subjects this thesis can benefit people responsible for analysis and design.

1.2 Literature Review

In this section, vibration control studies for offshore structures and time series forecasting are mentioned. The studies were classified as passive, active, semi-active, and hybrid, as explained in the following sections. Various researches have been conducted about the passive control system, which is one of the first control systems. The studies carried out are shown below.

In the study of Ou et al. performed in 2007, the vibration mitigation in the structure was investigated numerically and experimentally by using a damping system consisting of a rubber bearing and viscous fluid damper [3]. First, a study was carried out to find the optimal values for the damping systems [3]. It is assumed that the mass of the structure used in the study is lumped, and it has a single degree of freedom [3]. However, if the damping system is added to the structure, it is assumed that the structure has two degrees of freedom [3]. Glacial load and seismic induced forces affecting the structure were determined. A 1/10 scale model of the platform used in the study was created [3]. As a result of the experimental study on the shaking table, the properties of both rubber bearing and viscous fluid dampers were examined, and their effects on vibration reduction were investigated [3]. Afterward, a numerical solution was studied [3]. In the study, the displacement of the jacket platform, the inter-story of

isolate level, and the acceleration values on the deck were examined [3]. El-Centro, Traft, Kobe, and Tianjin earthquakes were applied to the system [3]. In line with the results obtained, it has been seen that the damping system gives effective results [3].

In the study of Patil and Jangid [4], the wave force acting on the jacket platform was tried to be controlled and reduced by using viscoelastic (VE), viscous, and friction dampers [4]. The damping capacities of three different dampers were compared. The wave force acting on jacket platforms with multiple degrees of freedom was calculated using the Pierson-Moskowitz spectrum and the Morison equation [4]. While the VE and viscous dampers were placed in the structure with the same method, the friction damper was added to the structure with a different method [4]. It has been seen that VE dampers give more effective results because they affect the lateral stiffness of the structure [4].

In the study of Chandrasekaran et al. performed in 2013 compare the vibration control results of tension leg platforms (TLP) using one tuned mass damper (TMD) or multiple TMDs [5]. For this, the parameters of the TMD system to be used were determined by using the H_2 algorithm [5]. Then, the Pierson-Moskowitz spectrum and Morison equation were used to calculate the random wave load [5]. The surge motion of the TLP was examined. It has been observed that the TMD structure performs efficient vibration control under extraordinary conditions [5].

After passive control systems, literature studies on time series prediction are mentioned.

In the study of Han et al. [6], a literature review was conducted for time series prediction studies using deep learning algorithms. First, the subclasses of time series prediction and deep learning algorithms used for time series prediction are explained [6]. In order to compare the described deep learning algorithms, a comparison was made using time series examples [6]. Also, error analyzes were performed to determine the accuracy of the predictions made [6]. The analysis results show that the LSTM algorithm's error value was lower than the error value of other deep learning algorithms in most of the studies [6].

In the study of Gensler et al. [7], solar energy forecasting was made using

physical photovoltaic forecasting model (P-PVFM), Multilayer perceptron (MLP), Autoencoder (AE), LSTM, and Deep Belief Networks (DBN) [7]. In this way, comparisons were made with the predictions made by Artificial Neural networks (ANN) and physical models [7]. In the study, forecasting was made with MLP, LSTM, and DBN. In addition, the neural network architecture created by combining AE and LSTM algorithms was compared with other neural networks [7]. It was seen that the error value of the neural network architecture obtained as a result of combining the AE and LSTM was found to be less in most studies [7].

In the study of Chimmula and Zhang performed in 2020, a trend prediction of the COVID-19 disease was made using the LSTM algorithm [8]. In addition, a forecast of when the disease will end in Canada and the world has been made. For this, firstly, publicly available datasets were used [8]. Then, the obtained data were forecasted using the LSTM algorithm. In addition, the values in Italy and America were also compared in the study [8]. It was concluded that the COVID-19 epidemic would end within three months from the date of the study [8].

1.3 Hypothesis

In the previous section, vibration controls using the passive control system and time series forecast studies using deep learning are explained. According to the studies, various spectrums and the Morison equation were used to calculate the wave forces that cause wave-induced vibrations. In this way, the wave force acting on the structures could be calculated. In addition, thanks to time series forecast studies, it has been seen that the value of any parameter in the future time step can be forecasted using the past and present time values. According to the results of the studies, it has been seen that the value of the wave force acting on the structure can be forecasted in the future time step by using the values in the time step. In line with this idea, if the value of the wave force in the future can be forecasted, the vibration can be reduced by applying a force to the system in the opposite direction of the forecasted wave force.

For this reason, as mentioned before, the aim of the thesis is to reduce the total force acting on the structure by direct feedback and to control vibration by forecasting the wave force acting in the opposite direction using the LSTM algorithm. In this way,

by controlling the vibration in the structure, it is ensured that the structure is protected from the wave force.

2. OFFSHORE PLATFORMS

Offshore platforms are divided into fixed platforms, compliant platforms, and floating platforms. This section gives information according to the purpose of usage, advantages, and disadvantages of offshore platforms.

2.1 Fixed Platforms

Fixed platforms were one of the first platforms used offshore. When they were first designed, they were used shallow water. In the process of time, they were used in deeper water. Two fixed offshore platforms are described. The first one is the gravity platform, and the second one is the jacket platform.

2.1.1 Gravity platforms

Gravity platforms are built to extract, store, or drill natural gas and crude oil. For this reason, their use in the sector is widespread [9]. The difference between the gravity platform is that it uses its weight to stay in its position [10]. In this way, it is useful in regions with connection problems to the sea bed [10]. The foundation design and of gravity platforms is a critical issue because it is expected to provide the necessary weight and cover a large area on the seabed [10]. In this way, it contributes to the system's stability and prevents the platform from overturning [10]. Gravity platforms can be constructed using both reinforced concrete and steel. The gravity platform built-in Nigeria can be an example of gravity structures made using steel [10]. The weight of the platform is 112,000 ton and the height of the platform is 241 m [10]. There are several advantages that gravity platforms have. The gravity platforms can be built fast [10]. In addition, gravity platforms can be installed on land and transported to the area where they are used [10]. However, it is inconvenient to use unsuitable soil for carrying loads [10]. As the construction continues, the start of operation may be delayed [10].

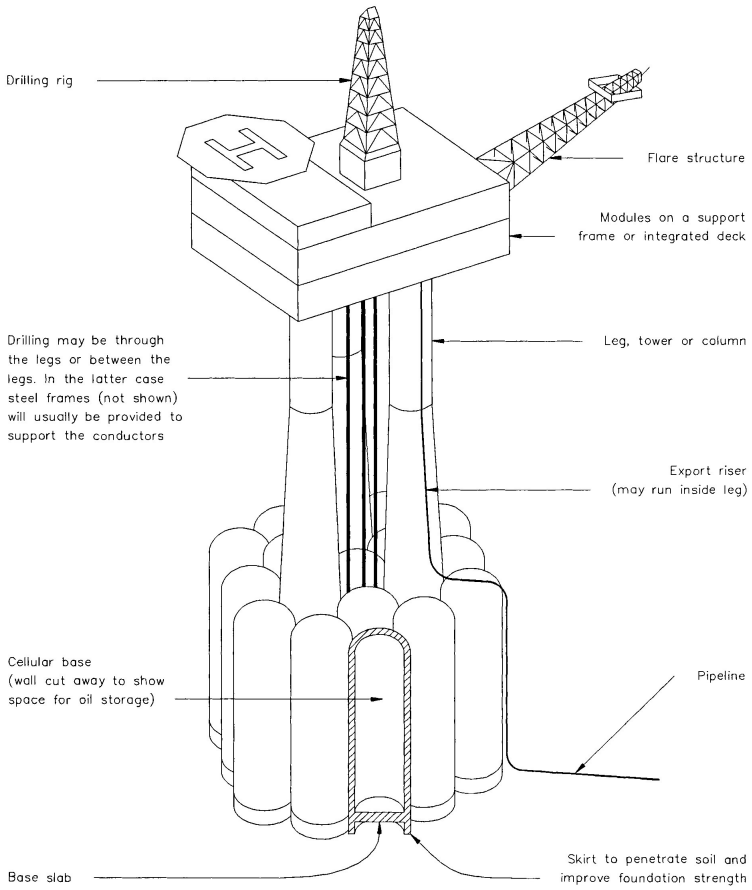

Figure 2.1 : Concrete gravity platform [11].

2.1.2 Jacket platform

The jacket platform is the second fixed platforms. The first steel jacket platform was built in 1947, and the water depth at the location where it was built was 20 ft [9]. However, over time, jacket platforms began to be used at deeper points, approximately 300 meter [9]. The weight of jacket platforms is also increased in time [9]. While the weight of the first constructed platforms was less than 1000 tonnes, it reached 46000 tonnes over time [9]. Jacket platforms have three components. These are piles, deck, and jacket [3]. There are several advantages to using jacket platforms. First of all, thanks to the pipes used, their stability is good [10]. They are suitable platforms for long-term production [10]. Not being affected by the scour on the seafloor and the high load-carrying capacity of the deck can be given as examples of its advantages [10]. However, jacket platforms are non-reusable platforms [10]. The initial and maintenance cost is high [10]. Corrosion can occur due to contact of the

steel on the platform with water [10]. So, the lifetime of the material used is reduced. As the depth increases, the cost increase is high [10].

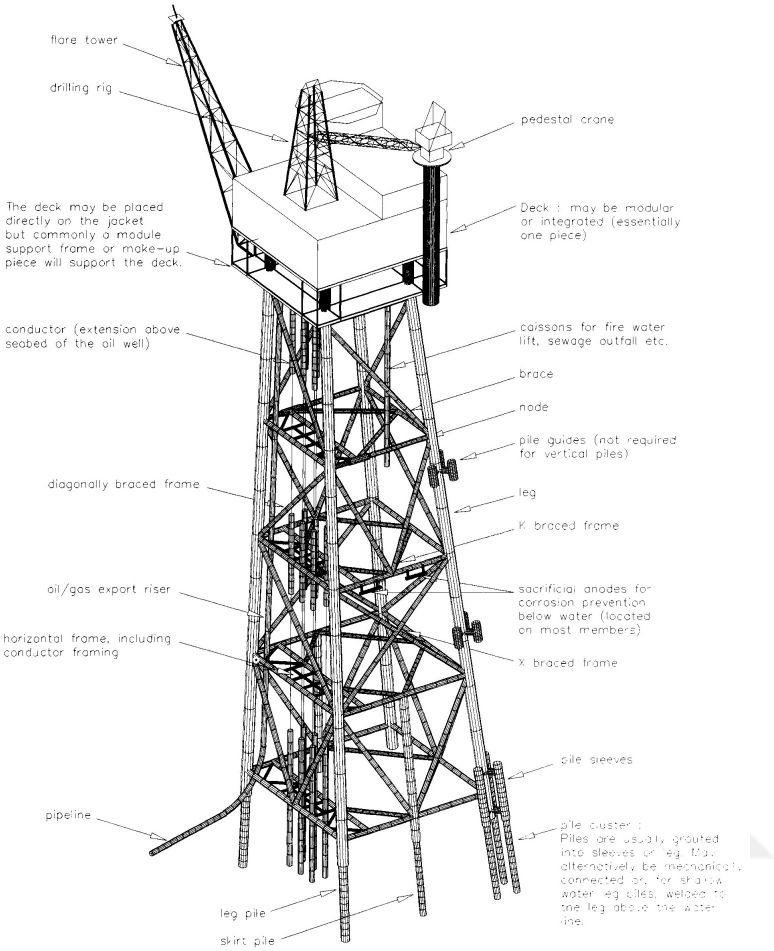

Figure 2.2 : Jacket Platform [11].

2.2 Compliant Platforms

Compliant platforms are the second offshore platforms. Due to the developments, it has been seen that compliant platforms are used instead of fixed platforms at deeper points [12]. Compliant platforms are offshore platforms designed to remain flexible with external factors [10]. There are three compliant platforms: guyed tower, articulated tower, and TLP.

2.2.1 Guyed tower

Guyed towers are the first compliant offshore platforms. These towers are tried to be kept in the region by using the guylines attached to the seabed [10]. The guy wires

consist of two parts, the upper part consists of a lead cable, while the lower part consists of a heavy chain [10]. The first guyed tower was installed in 1983 [10]. This tower, built at a water depth of 300 meters and has 12 buoyancy tanks [10]. In order to keep the tower in its position, approximately 20 guylines are attached to the tower [10]. The cost of guyed towers is not expensive [10]. Guyed towers have a good balance and can be reused [10]. However, the maintenance costs are high in contrast to the low costs [10]. The mooring required for the tower to remain in its position is difficult [10]. As the depth increases, the cost increase is high [10]. Guyed tower can be used in small areas [10].

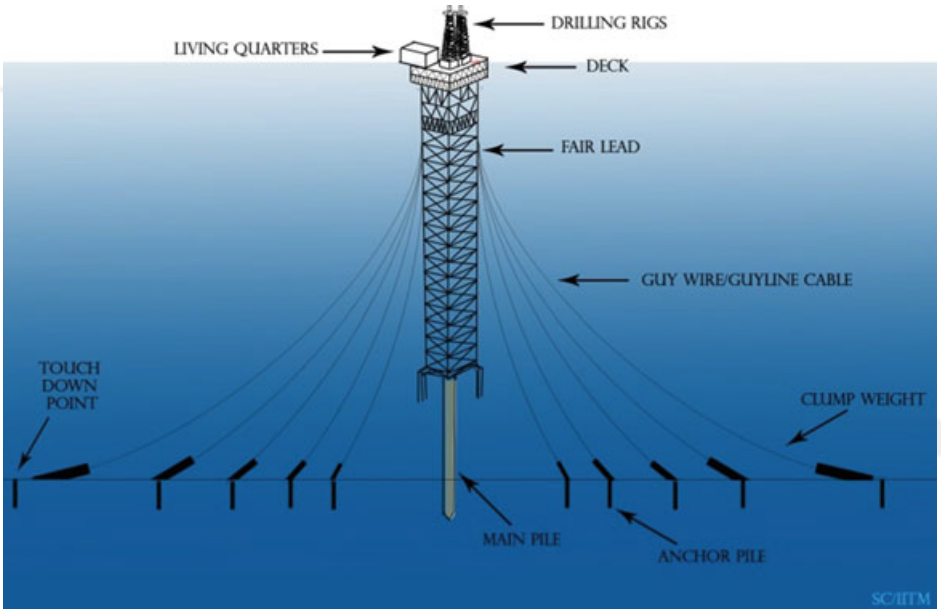

Figure 2.3 : Guyed Tower [10].

2.2.2 Articulated tower

Articulated towers are compliant offshore platforms articulated from their universal joint to their location [10]. The tower can be rotated freely around the base thanks to the universal joint [10]. The first articulated tower was built in 1963 [13]. It was initially designed for shallow waters. However, over time it could also be used at deeper points [10]. The depth of the area that can be used varies between 100-500 meters [14]. Another point to be considered in the design of articulated towers is that their natural frequency must be below the wave frequency [14]. The cost of articulated towers is not expensive [10]. However it can only be used in shallow waters. The design of the joints

is also a significant issue, and fatigue in the joint can cause difficulties in using the tower [10]. The use of the articulated tower is dependent on weather conditions [10].

2.2.3 Tension leg platform

TLP are one of the compliant offshore platforms, and it uses connections called tendons that help them stay in position [10]. In this way, while the vertical motion capacity of the platform is restrained, the horizontal motion capacity of the platform is compliant [10]. Usually, after a TLP is manufactured, it is placed on top of the system installed on the seabed before it was manufactured [10]. TLP is not expensive to maintain, and it can be reused [10]. As the depth increases, the cost increase is low [10]. The disadvantages of TLP are that the underwater parts of TLP are difficult to maintain [10]. The storage capacity of the platform is low [10]. The initial cost required for the platform is high [10].

2.3 Floating Platforms

Floating platforms are offshore platforms that can be used at deep points as they can float on the sea. Floating platforms are divided into subgroups semisubmersible, SPAR, floating production storage offloading (FPSO), floating storage offloading (FSO), and floating production system (FPS).

2.3.1 Floating production, storage and offloading system

FPSO is ship-shaped floating offshore platform [17]. Hydrocarbon production can be made by using FPSO [17]. Also, it is possible to store crude oil and offload it to other vehicles [17]. FPSO was formed by combining the first letter of the terms floating, production, storage, and offloading, respectively, to describe the platforms [10]. Apart from FPSO, FSO can store, offload, and FPS that do not have storage capabilities [10]. FPSO can be moved to the desired location [10]. In addition, it can be reused [10]. The cost of the FPSO is low [10]. It requires less infrastructure [10]. One of the most important advantages is that it is easy to disconnect the connections that allow it to stay in the region [10]. In this way, problems encountered, especially in the glacial area,

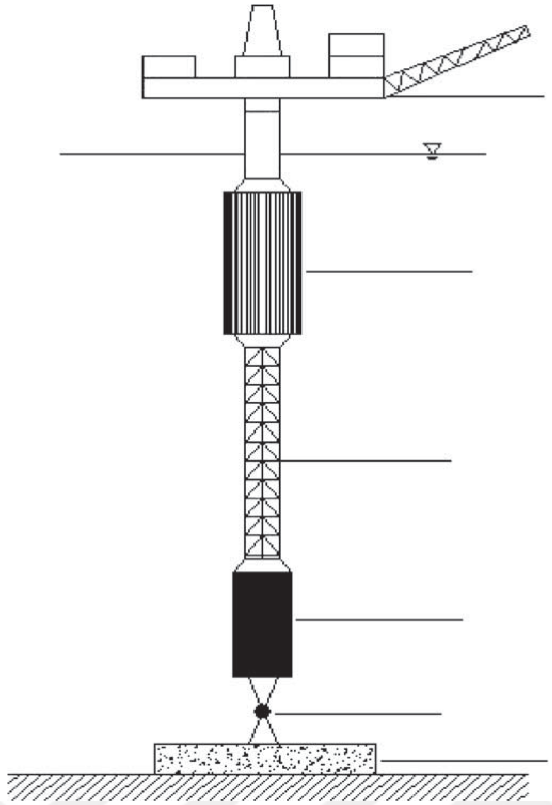

Figure 2.4 : Articulated Tower [15].

have been prevented [10]. FPSO platforms are insensitive to depth [10]. However, it is not stable in rough seas [10]. The load capacity and oil storage capacity that can be carried on the FPSO's deck are limited [10]. In addition, the use of the FPSO is limited to small areas [10].

2.3.2 Spar platform

The second floating offshore platform is spar. It was first installed in 1997, and the purposes of usage are drilling and production [17]. Spar has four components—the hull, topside, riser, and mooring system [17]. The specific part of spar is the hull part, and it is aimed to reduce the effects of currents by encircling the hull with a helical strake [17]. In addition, thanks to the design of the hull part, it can be stable [17]. The traditional mooring method is preferred for spar to connect the seabed [10]. Three types of spar platforms exist classical spar, truss spar, and cell spar [17]. Spar has several advantages. The platform can remain stable even if the mooring system is disconnected [10]. Also, spar allows production on the surface [10]. Spars are easy

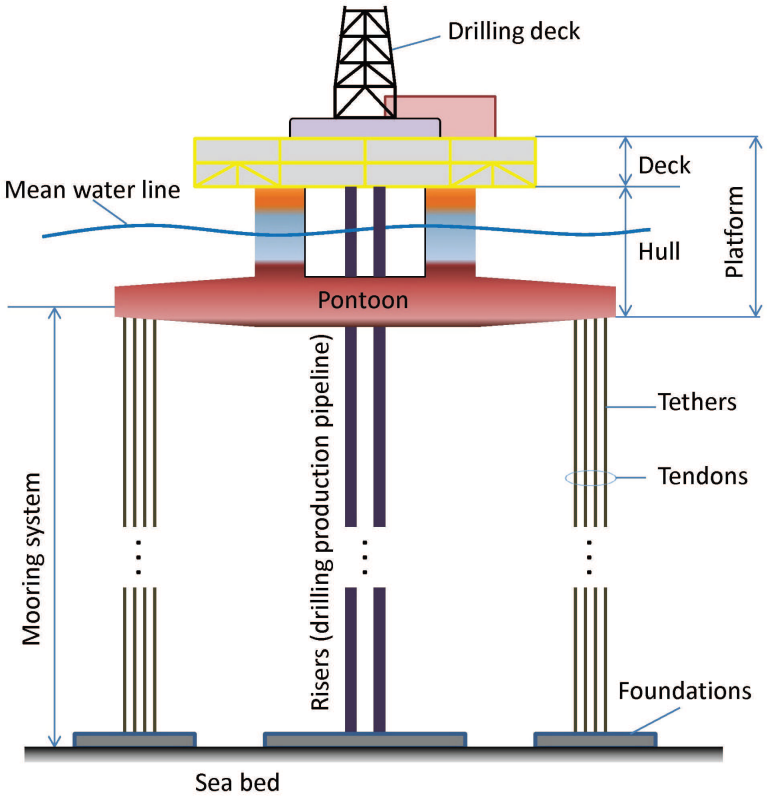

Figure 2.5 : Tension Leg Platform [16].

to fabricate [10]. The pitch and heave movements of the spar are low [10]. The disadvantages of spar are there are no drilling facilities, and it has limitations for storage [10].

2.3.3 Semisubmersible

The type of floating offshore platforms is semisubmersible. Semisubmersible is used in the oil and gas industries [10]. The most important feature is that it stands still by showing minimum movement against external loads [10]. Semisubmersible can only be moved by towing [10]. Semisubmersible have four components: pontoons, columns, deck, and mooring lines [10]. The pontoons keep the platform above the water, and columns support the deck and contribute to the work on the deck [10]. Semisubmersible is very good at standing in balance as they have less response to wave motions affecting the platform [10]. In addition, it can be moved to another region, and its transportation speed is high [10]. Another advantage is that the semisubmersible has more deck area [10]. However, unlike the previously mentioned deck area, the

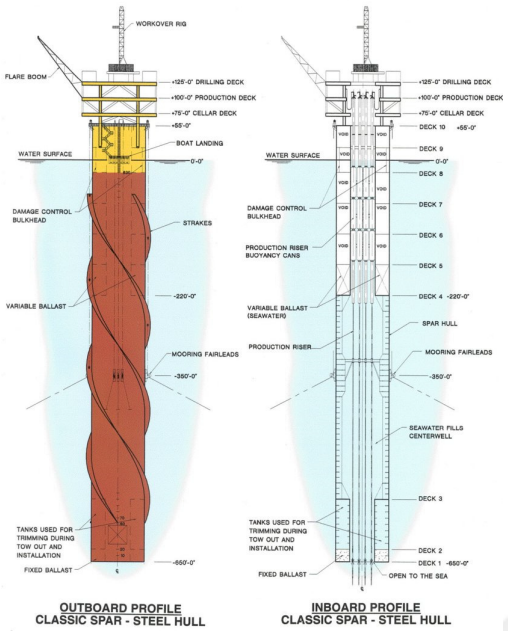

Figure 2.6 : The Classic Spar Platform [18].

amount of load carried on the deck is limited [10]. The transportation costs of the platform that can be moved to the desired region are high, and the mooring system is challenging to use in rough seas [10]. The initial cost and operating cost of the platform are high [10].

3. VIBRATION CONTROL OF OFFSHORE PLATFORMS

This section gives information about vibration control systems in the literature and vibration control studies in offshore structures.

3.1 Types and Dynamics of Vibration Control

Vibration control systems are divided into four subclasses in the literature. These are passive control systems, semi-active control systems, active control systems, and hybrid control systems.

3.1.1 Passive control

The passive control system controls the vibration occurring in a system without external power [19]. In order to control vibration, a building can be isolated from external effects, can be protected by dissipating the energy, or the dampers inside the building can absorb energy. Three basic methods are explained.

3.1.1.1 Base isolation

Base isolation is one of the passive control used for vibration control. Base isolation began to be used in civil engineering in the 1960s [20]. Its working principle is to isolate and protect the structure against external factors using base isolation. In this way, the structure is less affected by external factors. With base isolation, a structure becomes vertically stiff and horizontally more flexible [21]. In order to increase the seismic resistance of the building designed in structural engineering, it is to minimize floor accelerations and interstory drift [21]. Another fundamental problem encountered in structural engineering is the rigidity of structures [21]. If the structure's stiffness is high, the floor acceleration is higher [21]. On the other hand if the structure is very flexible, interstory drift is high and damages the structure [21]. A base isolator can be used to avoid this problem [21]. The required values are provided using the base isolator, thus minimizing floor acceleration and interstory drift [21]. Studies show that

the base isolation method provides highly effective protection against external factors affecting the structure [22].

3.1.1.2 Metallic yield damper

Metallic yield dampers are dampers that control vibration by dissipating energy [19]. It dissipates the energy by using the inelastic deformations of the metals [19]. The characteristic features change according to the material used in metallic yield dampers [23]. Metallic yield dampers can be classified under four primary materials. These are steel dampers, aluminum dampers, lead dampers, and copper dampers [23]. Metallic yield dampers are reliable [23]. They are not sensitive to temperature, and they have stable hysterical behavior [20]. However, since metallic yield dampers do not show linear behavior, their analysis and design are not easy [20]. Metallic yield dampers are not effective at dissipating energy when first used [20]. It appears to dissipate energy when large inelastic deformations occur [20].

3.1.1.3 Friction dampers

Friction dampers are dampers that create friction by sliding over each other to provide energy dissipation [20]. Friction dampers, which have been used in brake systems in the automotive industry for a long time, are also used in structural engineering [19]. The friction dampers is widespread due to their economic, effective and reliable [20]. It is difficult to use the mechanical properties of friction dampers throughout their lifetime [20]. Although it is easy to install, it is not easy to analyze and design due to its nonlinear behavior [20]. The effects of external factors such as temperature and corrosion, a decrease in damping capacity can be observed [20].

3.1.1.4 Viscoelastic dampers

VE dampers, one of the passive control, dampers by converting mechanical energy into heat energy [24]. It controls vibration by using VE materials that contain shear deformation [20]. Examples of VE materials are polymer and rubber [20]. When shear deformation occurs between the plates due to the force acting from the outside, it is seen that the energy is dissipated by the VE dampers [20]. The advantages of VE

dampers are their linear behavior [20]. In this way VE dampers are extremely easy to analyze and design [20]. However, VE dampers are more affected by temperature changes [24]. Another disadvantage is that they may encounter various problems due to their high stiffness [24].

3.1.1.5 Viscous fluid dampers

Unlike other energy dissipation methods, viscous fluid damper uses fluids to dissipate energy. Like VE dampers, it dissipates energy by converting mechanical energy into heat energy [24]. Viscous fluids are often used for vibration reduction in the aerospace industry and the military [25]. A piston in the system moves the viscous liquid [20]. The motion of the viscous liquid converts mechanical energy into heat energy [20]. Viscous fluid dampers show linear behavior [20]. However, their efficiency may vary depending on temperature and frequency [20].

3.1.1.6 Tuned mass dampers

TMD is the first energy absorber mechanism consisting of a viscous damper mechanism, a mass, and a spring [22]. TMD uses its mass to absorb energy. When external force act in structure, the mass inside of the TMD begin the motion on the counter phase [26]. After the movement, TMD generates the control force to dampen the vibration [26]. TMD is simple, reliable and the maintenance is easy [26]. Also, there is no need external power source to control the structure [26]. However, TMD is effective only in single mode [20]. Moreover, in case of limited space, there may be a need for space [20].

3.1.1.7 Tuned liquid dampers

Tuned liquid damper (TLD) is a second energy absorber mechanism. For the first time, TLD was used in ships to mitigate vibration [26]. After that, TLD was used in civil engineering [26]. TLD is similar to TMD, but there are a few differences. One of the differences is that TLD uses water or another liquid as a mass. When the external force acting structure liquid begins the motion in TLD, energy is absorbed by generating friction between liquid and container [20]. Also, the turbulence of fluid

motion is another damping factor [20]. This section describes two different types of TLD. The first one is a sloshing damper [20]. The sloshing dampers can dampen using the movement and depth of the liquid and the size of the container it contains. The second one is a tuned liquid column damper (TLCD) [20]. Air pressure and columns are used to adjust the natural frequency of the TLCD [20]. TLD is highly effective against vibration from any direction when lateral vibration affects the system [20]. Moreover, TLD can be used as a water supply [20]. Then it can be helpful in a fire. In addition, TLD is convenient for cost and maintenance [26]. On the other hand, TLD is not as effective as TMD [26]. Because the density of water used in TLD is less than the steel used in TMD [26]. Also, the behavior of TLD is nonlinear [20]. For this reason, the design of TLD is complicated [20].

3.1.1.8 Advantages and disadvantages

Passive control is used in many places today. Reliability and economically viable are some of the features that highlight its use [27]. In addition, it seems that they are practical than other control systems since they do not use any control mechanism or electronic system [27]. However, it does not change the reaction when faced with unstable situations is one of the disadvantages [27].

3.1.2 Semi active control

Semi-active control system is a system developed to control the damping properties of passive control [20]. It performs vibration control with its passive control device in semi-active control systems [20]. However, unlike passive control, it performs vibration control more effectively by adjusting the behavior of its passive control device by measuring external factors or the reaction of the system to external factors [20]. The required energy can be provided by using batteries [28]. The semi-active control system consists of four main components [20]. The first components are sensors. The sensors measure the external effects or the structure's reactions against external effects [20]. The second component is the control computer, which generates the signal to provide the signal which is necessary for vibration control [20]. The third component is the passive device [20]. The passive device is used for vibration

control [20]. The last component is the actuator. The actuators contribute to the vibration control of the system by adjusting the behavior of the passive device in the system [20]. Semi-active control systems are described below.

3.1.2.1 Semi active tuned mass damper

Semi-active tuned mass dampers were used in 1983 [29]. The system is developed to protect the structure from the effect of the wind. In order to do this, it is positioned in the upper part of the structures. The system consists of TMD and an actuator. It controls vibration by controlling the damping capacity of TMD [20]. Since the mass of the TMD is less than the mass of the building and the actuator changes the damping capacity of the TMD instead of applying control force, it requires less energy [20]. Thanks to using of actuator optimally, the mass of the TMD is efficiently moving [20].

3.1.2.2 Semi active tuned liquid damper

Unlike the passive system, it allows the natural frequency of the system to be kept at the optimal value by changing the motion of the liquid in TLD [20]. In order to change the motion of the liquid in the system, the features of the system are used. One of these features is that if the system has an orifice opened and closed to provide liquid flow, liquid flow can be controlled using these orifices [20]. Another example is the control by changing the direction of fluid or direction of the pipes in which the liquid moves [20]. In this way, it is seen that it is more efficient than passive control. The low cost required to achieve the desired yield is also noteworthy as one of the reasons for option.

3.1.2.3 Semi active stiffness control devices

One of the semi-active control system is semi-active stiffness control devices that allows the structure's stiffness to be adjusted [28]. Thanks to the devices placed in the bracing system of the structure, stiffness control can be done [20]. Resonance effects are minimized by using semi-active stiffness control devices [20].

3.1.2.4 Semi active friction damper

One of the semi-active controls is the semi-active friction damper. It is aimed to dissipate the energy. However, unlike the passive system, the desired damping is achieved by controlling the friction and damping with the control system [20]. In this way, the protection of the system is ensured. It is an advantage that low energy is required for the system to work [20].

3.1.2.5 Electrorheological fluids

Electrorheological (ER) fluids are smart fluids in which rheological properties change due to the external electric field effect [30]. Viscosity, yield stress, and shear modulus can be given as an example of these properties [30]. When the electric field affects the system, a change begins to occur in the fluid, and because of this change, the fluid shows semi-solid properties [20]. The adjustable electric field allows the damping capacity to be increased or decreased [20]. In this way, ER fluids can be used more effectively due to controlling the system [20]. On the contrary, the advantages of ER dampers, the yield stress of ER dampers is low [20]. Also, the high voltage required for the ER fluid [20]. One of the factors that limit the usage is that it creates a safety problem resulting from the use of high voltage, and it is not economically viable [20]. In addition, the sensitivity of ER dampers to pollution is another factor affecting the system [20].

3.1.2.6 Magnetorheological fluids

Magnetorheological (MR) fluids are one of the smart fluids that can be used for vibration control. It changes the characteristic features of the system due to the influence of the magnetic field [31]. As a result of the influence of the magnetic field, the particles in the fluid pass into chain form, allowing the liquid to show the properties of non-Newtonian liquids [31]. In this way, it performs vibration control. Because of removing the applied magnetic field, the system starts to show the properties of the Newtonian fluid again [31]. These changes can be measured in milliseconds [31]. Due to the advantages of MR fluids, the usage area is extensive. One of the examples of the advantage is, it can be used in the range from -40 degrees Celsius to 150

degrees Celsius [32]. In addition, being insensitive to the pollution of the fluid and obtaining high efficiency at low cost can be given as examples of other advantages [33]. However, its nonlinear behavior can be given as an example of its disadvantages [33].

3.1.2.7 Semi active viscous fluid damper

Another semi-active control system is the semi-active viscous fluid damper. According to semi-active viscous fluid damper, energy dissipation can be made due to the fluid passing through the valve [20]. It is seen that these systems, which dissipate energy through friction, provide the desired efficiency thanks to the control algorithms [20]. In order to achieve the desired efficiency, the control algorithm adjusts the openings of the valve in the system [20]. When the opening in the valve is small, the damping is more because the fluid movement is difficult [20]. If the opening in the valve is large, the damping is less [20].

3.1.2.8 Advantages and disadvantages

The amount of energy required to use the semi-active control system is low, and therefore, the required energy can be satisfied by using the battery [20]. The problems that may occur since the disconnection with the energy source encountered inactive control are prevented by using the battery [20]. Some of the advantages of these systems are that it is more efficient than the passive control system, and it is reliable and easy to maintain [20]. However, they are more complex systems than passive control system, and limited control capacity is also one of its disadvantages [20].

3.1.3 Active control

Active control is a control system developed to solve the problems of passive control system and semi-active control system [20]. As the passive control system cannot adjust the control capacity, and the effectiveness of the semi-active control systems is as much as the efficiency of the passive system, it has been started to work on a new control system that can provide control in the wide frequency band [20]. This new control system is the active control system. The active control system contains a sensor, an actuator, and a controller [20]. The sensors are the unit that measures the

external effects or the values such as displacement, velocity, and acceleration due to the external effect of the structure and sends it to the controller [20]. The controllers are the device that evaluates the external factor affecting the structure and generates a control signal using the previously determined control algorithm, and transmits it to the actuator [20]. The actuators are the device that creates the control force by using the control signal from the controller [20]. The active control system can be examined under three sub-topics. These are active mass damper (AMD), active tendon systems and pulse generation systems.

3.1.3.1 Active mass damper systems

AMD is one of the control systems studied since the early 1980s to provide control in cases where TMD is insufficient [20]. If the first mode of structure is dominant, then TMD can effectively control the vibration [20]. However, it is less effective in controlling vibration in other modes [20]. It is seen that control can be made in a wide frequency band by using AMD [20]. Vibration control is provided by placing the control actuator between the TMD and the structure [34]. It is moved TMD according to the control algorithm of the system [34]. There are economic benefits resulting from mitigating the vibration by controlling the movement of the auxiliary mass [34]. Thus, it uses less control force than active control systems affecting the structure [34]. However, although AMD is effective against the fundamental frequency, it is not effective against higher frequencies [20].

3.1.3.2 Active tendon systems

Active tendon control systems, one of the active control approaches, consist of pre-tensioned tendons [20]. The tensions of these pre-tensioned tendons can be controlled [20]. One end of these control systems placed between two floors is connected to the upper floor, and the other is connected to the actuator providing the control located on the lower floor [20]. It is seen that the control is provided thanks to the adjustment of the tension in the tendons [20]. One of the advantages of active tendon control systems appears to be highly efficient in seismic control [20].

In addition, it is seen that active tendons can protect against both impact and external forces acting for a certain period [20].

3.1.3.3 Pulse generation systems

The third active control system is the pulse generation system. For vibration control, pulse generators can place many places in the structures [20]. In case of occurrence of relative velocity in any position where the pulse generators are placed, vibration control is performed by creating a control force by the system [20]. Pulse generation systems are cheap [20]. It also uses compressed gas to control vibration [20]. Therefore, it may not be sufficient for vibration control [20].

3.1.3.4 Advantages and disadvantages

As mentioned before, the active control system solves the problems passive and semi-active control systems face. The main ones are that the control capacity of the system can be increased. Especially in today's world, due to the development of technology, the desired efficiency can be achieved thanks to the production of advanced control systems. Active control systems can evaluate external factors and perform control accordingly [20]. In addition, it is possible to control in a wide frequency range by using the active control system [20]. However, contrary to its technology, it is still a new field, so research on it still needs to be done.

3.1.4 Hybrid control

The previous section stated that active control is a system developed to eliminate the disadvantages of the passive control system and semi-active control system [20]. However, active control also has several disadvantages [20]. For this reason, a fourth control system has been developed [34]. This system is called hybrid control. Hybrid control system has been investigated in the 1990s [34]. It includes the advantages of other systems [34]. The hybrid control has been classified under three main subtopics. These are the hybrid mass damper (HMD), the hybrid base isolation, and the hybrid damper-actuator bracing control [20].

3.1.4.1 Hybrid mass damper

HMD, which is the combination of an active control actuator, and a TMD, is one of the hybrid control systems frequently used in civil engineering [19]. The vibration reduction capacity of the HMD control system depends on the movement capacity of the TMD inside the HMD [20]. Less energy is consumed than AMD [20]. It is possible to increase the efficiency of HMD by using an actuator. In this way, the limitation of TMD can be solved. However, if there is an area limitation in the region where it is located, there may be problems in terms of usage [20].

3.1.4.2 Hybrid base isolation

Hybrid base isolation is one of the hybrid control systems developed by combining the base isolation and an active control system [20]. Base isolation is placed between superstructure and foundation. The active tendon is placed on superstructure [20]. Its usage is restricted because the base isolator cannot change the control capacity against external factors [19]. However, the control capacity can be increased if an active control system is added to the base isolator [19].

3.1.4.3 Hybrid damper-actuator bracing control

Hybrid damper-actuator bracing control systems are hybrid control systems. It is formed by combining active and passive control systems. The passive device for passive control can be spring dampers, viscous fluid dampers, or liquid mass dampers [20]. As an active device, hydraulic actuators can be used [20]. Both theoretical and experimental studies were carried out for hybrid damper actuator bracing control systems. Hybrid damper actuator bracing control has the advantages. The control capacity of hybrid damper-actuator bracing control systems is higher than HMD systems [20]. In addition, the cost is more affordable than the hybrid base isolators [20].

3.1.4.4 Advantages and disadvantages

The hybrid control system is a new system that includes the advantages of passive, active, and semi-active control systems that have been mentioned before. Hybrid control systems contain a passive system that is reliable and an active control system that is high control capacity [20]. In this way, it closes the gaps by using the advantages of the other system at the points where the systems are lacking. The hybrid control system is more effective than the passive control system [20]. In addition, the control capacity is higher [20]. Also it is more cheap than active control system [20]. In the previously mentioned semi-active control system, since only the damping feature of the passive control can be adjusted, the control capacity of the active control cannot be used. Unlike semi-active control systems, in hybrid control systems, the control force created by active and passive systems can be used to reduce vibration [35]. Consequently, the hybrid control system seems extremely useful for vibration control.

3.1.5 Control strategy

This section describes the control strategies used for vibration control.

3.1.5.1 Feedback control

In this section, feedback control applied for vibration control is explained. The feedback control strategy controls the vibration in the structure by giving the force called the control forces acting on the system [36]. The equation of feedback control is shown in Equation 3.1.

$$[M]\{\ddot{q}(t)\}+[C]\{\dot{q}(t)\}+[K]\{q(t)\}=\{F(t)\}+\{F_D(t)\} \tag{3.1}$$

Parameters specified as M, C, K are mass damping and stiffness matrices, q, $\dot{q}$, and $\ddot{q}$ are displacement, velocity, and acceleration respectively, F indicate external force finally, F_D indicate control force. This study carried out vibration control using the feedback control strategy. For this the F parameter represents the wave loads in the two different studies that have been explained later. The feedback control force shown in F_D is the wave loads forecasted using the LSTM algorithm, explained in the next

section. After forecasting the control force's value, it aims to control the vibration by affecting the wave load in the opposite direction as feedback to the system.

3.1.5.2 State variable feedback control

In this section, the state feedback control approach is explained. According to this control approach, vibration control is attempted by using the displacement and velocity values of the system during vibration. Vibration control is performed as a result of giving feedback to the system by multiplying the displacement and velocity values determined as state variables with coefficients [37]. The state variable feedback control strategy is demonstrated in Equation 3.2.

$$M\ddot{\mathrm{q}} + (C+G)\dot{\mathrm{q}} + (K+H_D)\mathrm{q} = -K_p\mathrm{q} - K_v\dot{\mathrm{q}} + \mathrm{F(t)} \tag{3.2}$$

In Equation 3.2, K_p and K_v are called feedback gain matrices, G is gyroscopic matrix, H_D is circulatory matrix. In the control approach, as seen in Equation 3.2, the displacement value is multiplying with K_P and the velocity value is multiplying with K_v value and given as feedback to the system. In this way, it is aimed to reduce the vibration that occurs in many systems.

3.2 Types and Dynamics of Vibration Control of Offshore Structures

In the previous sections, studies using passive control systems were explained. In this section, vibration control studies of offshore structures using semi-active, active, and hybrid control systems are explained.

Caterino [38] carried out an experimental study using the MR damper to reduce the vibration in the wind turbine [38]. For this, a wind turbine scaled to 1/20 was used. Then, after the characteristics of the MR damper and sensors to be used in the experiment were determined, the experimental study was started [38]. Two different wind loadings and two different control algorithms were compared [38]. In the experimental study, the displacement and base stress values in the structure in which the fixed-based and semi-active control systems are compared under two different wind

loads [38]. In addition, the performances of the control algorithms were also evaluated in the study [38].

The study by Leng and Xiao [39], it was tried to control the vibration that occurs in the offshore structure as a result of the wave-induced effect by making numerical calculations of the MR elastomer device [39]. After the test and performance evaluation of the MR elastomer device, the random wave load to affect was calculated using the Pierson-Moskowitz wave spectrum and linear Morison equation [39]. After calculating the dynamic response of the offshore structure using the finite element method, a study was conducted on the displacement, velocity, and acceleration reduction values of the structure as a result of horizontal and vertical placement with and without using a MR elastomer device [39]. According to the results obtained, it has been observed that the MR elastomer device reduces the displacement, velocity, and acceleration values in the structure [39].

Wang and Li [40] aimed to reduce the vibration in the steel jacket platform by using a semi-active control system in their study [40]. For this, MR damper and linear quadratic gaussian (LQG) approach are used. The equation of motion of the system was created with the MR damper. Then, a numerical study was done for both MR damper and LQG control systems [40]. The wave force acting on the structure was calculated by the linear Morison equation [40]. The sea state was determined by using the JONSWAP wave spectrum [40]. The control force values of the MR damper and the LQG control system were compared [40]. It was seen that the control force value of the MR damper was lower than the control force of the LQG control system [40]. Then, the study was carried out by combining the MR damper and the LQG control system [40]. In the study, the displacement and acceleration that occur due to the wave force acting on the structure, with and without the control system, were examined [40]. It was observed that the control capacity increased by combining the MR damper and the LQG control system [40].

Gattulli and Ghanem [41] tried to control vortex-induced vibrations by using adaptive control technique [41]. In order to control the vibration in the structure, an active control system has been installed that controls the movements of the mass in TMD [41].

The external force acting on the system is calculated using the Morison equation [41]. Thanks to the control algorithm used for vibration control, the control force is created by controlling the motions of the mass in the TMD [41]. In this way, it has been observed that the structure is controlled against vortex-induced vibrations [41].

Terro et al. [42] tried to control the jacket platform using multi-loop feedback control against wave-induced hydrodynamic force in their study [42]. The nonlinear wave force acting on the structure was calculated using the Morison equation [42]. Then, after determining the mechanical properties of the jacket platform, the properties of the multi-loop feedback control were determined [42]. Multi-loop feedback control consists of two different feedback loops [42]. The first of these is called the inner loop, and the second of these is called the outer loop [42]. Thanks to the inner loop, the system's stability against linear effects are ensured [42]. The system's stability against nonlinear effects is maintained thanks to the outer loop [42]. After the necessary preparations for the system were made, the uncontrolled and controlled systems were compared for every floor [42]. For this simulation, the SIMULİNK model is also used to show the response of the jacket platform's floors [42]. It was seen that multi-loop feedback control is beneficial for vibration control [42].

In the study conducted by Som and Das [43], MR dampers, which is one of the semi-active control systems, have been used to reduce the response of the jacket platform to earthquake-induced factors [43]. In addition, a decentralized sliding mode control approach and clipped-optimal control algorithm are also used [43]. Thanks to the Clipped-optimal control algorithm, the command voltage value to the MR damper can be generated [43]. In the study, the displacement value resulting from the use of the MR damper in different positions and quantities on the jacket platform was examined [43]. The displacement value on different floors was compared [43]. The displacement values resulting from applying different voltage values to the MR damper are compared [43]. In addition, in the study, the variation of displacement and control force values over time was compared by taking into account the cases where the drag force is linear, nonlinear, or there is no drag force [43]. In the study, it is seen that the response of the structure is reduced by using the MR damper [43].

The study conducted by Taghikhany performed in 2013, MR dampers, one of the semi-active control systems, and friction pendulum insulators are used to control the vibration of the Sirri jacket offshore platform against seismic factors [44]. First of all, the characteristics of the structure were determined [44]. Then, the control algorithm to be used in the system was determined [44]. For this, the H2/LQG algorithm was created [44]. Finally, the displacement and acceleration values were compared with and without the control system [44]. It has been shown that the semi-active control system is beneficial for vibration reduction [44].

4. VIBRATION CONTROL BY DEEP LEARNING TECHNIQUES

In this section, the usage and benefits of deep learning, the time series forecast by deep learning, and commonly used deep learning algorithms are explained. In addition, the structure and usage method of the LSTM algorithm, which is used for the study, is also explained.

4.1 Benefits and Usage of Deep Learning

Deep learning, which is a sub-branch of machine learning, is frequently used today. There are three reasons for the widespread use of deep learning. The first reason is the increase in the amount of data obtained [45]. The second reason is that better results can be obtained by using better equipment with the development of technology [45]. The third reason is the development or creation of algorithms used for deep learning [45]. In addition, it has been seen that deep learning gives better results against many of the limitations faced by artificial intelligence [46]. It is possible to see these limitations in traditional machine learning as well [46]. Some of the limitations machine learning faces require careful engineering and domain expertise [46]. However, unlike machine learning, deep learning performs the learning process using data thanks to the learning procedure [46]. In addition, unlike machine learning, deep learning automates feature engineering, which is one of the essential steps of machine learning [45]. In addition, the performance of solving the problems faced by deep learning is high [45].
Deep learning is used in many fields, such as image processing [47], speech recognition [48], and time series forecasting [6].

4.1.1 Time series forecast by deep learning

Time series are obtained by arranging the measurable observations according to the time step [49]. Using time series, the change of many data according to time can be examined and used in studies. Significantly, the forecast of the data in the t+h

step of the future time using the time series has made the time series forecasting more attractive. Thanks to the developments experienced today, more data can be accessed, and it has become easier to record data. Consequently, with the developments in artificial intelligence, time series forecasting is made efficiently. Finance [50], optimization, and programming are a few examples of areas where time series forecasting is used.

There are deep learning algorithms used for time series forecasting. Some of these are convolution neural networks (CNN), recurrent neural networks (RNN), LSTM, and DBN can be given as examples [6].

4.2 Common Deep Learning Networks

This section gives information about some of the most widely used deep learning algorithms [51]. These algorithms are CNN, RNN, DBN, and AE. Also, information about LSTM used in our study is given.

4.2.1 Convolution neural network

CNN, one of the most used deep learning algorithms. CNN is widely used in computer vision, image classification, and voice recognition areas where the image is used as data [52]. It contains four layers: convolutional layer, non-linearity layer, pooling layer, and fully connected layer [52]. Although there are parameters in the convolutional layer and the fully connected layer, there are no parameters in the other layers [52]. Its advantage over ANNs is that it reduces the number of parameters [52]. In this way, it can perform operations that ANNs have difficulty doing [52]. It was also seen that CNN was successful in solving the problems faced by machine learning [52].

4.2.2 Recurrent neural network

RNN was developed in 1980, and it is one of the most used algorithms in deep learning [53]. Because RNN uses serial data, it is widespread to use time series forecasting and natural language processing [53]. It can be said that the RNN has short-term memory due to its features [54]. Due to the feature of the RNN structure, vanishing gradient and gradient exploding problems can be encountered [54]. Unlike the traditional neural

network structure, the RNN structure can transfer information from the subsequent layers to the inputs by the feedback method [53]. In this way, when the RNN structure produces an output, it produces a value that affects its previous information [53].

4.2.3 Deep belief network

DBN was first defined as a stack of Restricted Boltzmann Machines (RBM) [51]. In this way, information capacity and abstraction ability are increased [6]. The previously mentioned stacked RBM layers are linked to the layers before and after [51]. It is used more frequently than the RBM algorithm for forecasting temporal data [6]. It can benefit from unlabeled data compared to traditional neural network architectures [55]. DBM creates a model for the system using both the unsupervised stage and the supervised stage [55].

4.2.4 Autoencoder

AE is a feedforward neural network model used for unsupervised learning [51]. AE reduces the dimensionality of the input data [56]. Then, it learns to reconstruct the input data in the output layer and provides its operations [56]. It uses two blocks called encoder and decoder for this [56]. AE has different processing capabilities than supervised learning using backpropagation since they try to reconstruct the input data [56].

4.2.5 Long short term memory

LSTM was developed to solve the exploding gradient and vanishing gradient problems encountered by RNN [57]. It is possible to avoid the problems encountered in classical RNN structures and use the gradient in long series data by using LSTM. In order to do this, the LSTM architecture includes memory cells and gates that allow the gradient to be transmitted in a controlled, updated, and forgotten. Formulas related to LSTM are given.

$$f_i^{(t)} = \sigma(b_i^f + \sum_j U_{i,j}^f x_j^{(t)} + \sum_j W_{i,j}^f h_j^{(t-1)}) \tag{4.1}$$

$$g_i^{(t)} = \sigma(b_i^g + \sum_j U_{i,j}^g x_j^{(t)} + \sum_j W_{i,j}^g h_j^{(t-1)}) \tag{4.2}$$

$$q_i^{(t)} = \sigma(b_i^q + \sum_j U_{i,j}^q x_j^{(t)} + \sum_j W_{i,j}^q h_j^{(t-1)}) \tag{4.3}$$

$$s_i^{(t)} = f_i^{(t)} s_i^{(t-1)} + g_i^t \sigma(b_i + \sum_y U_i x_j^{(t)} + \sum_y W_i h_j^{(t-1)}) \tag{4.4}$$

$$h_i^{(t)} = \tanh(s_i^{(t)}) q_i^{(t)} \tag{4.5}$$

The $f_i^{(t)}$ represents the forget gate, $g_i^{(t)}$ represents the input gate, q_i represents the output gate, $h_i^{(t)}$ indicates the hidden layer, $s_i^{(t)}$ indicates the cell state, and U, W, and b parameters are input weight, recurrent weight, and bias, σ is logistic sigmoid function [58]. The forget gate decides which information is forgotten [59]. A value of 0 indicates that the information is forgotten, and a value of 1 indicates that the information is kept in the system [59]. The input gate decides what information goes into the cell. It determines the hidden layer value that will be output from the cell using the data. U, W, and b parameters are used to calculate the value of gates and different values of these parameters are used to calculate every gate.

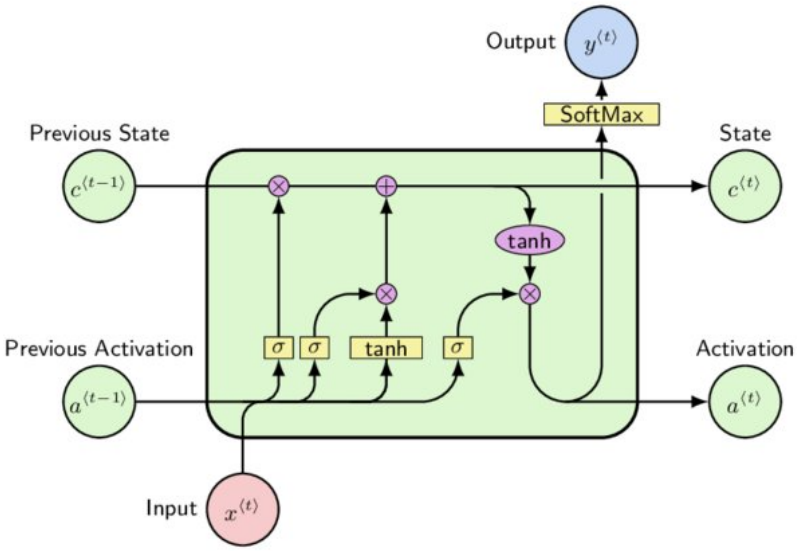

Figure 4.1 : The long short term memory cell structure [60].

4.3 Vibration Control via Deep Learning Techniques

The study of Lu et al. [61] aimed to increase the control capacity of the LQR control algorithm [61]. For this, the parameters of the LQR control algorithm were optimized by using a CNN and a genetic algorithm (GA) [61]. The CNN algorithm is used to identify the vibrations affecting the system [61]. After that, a study was conducted to evaluate the system's performance [61]. Optimization was performed according to each vibration type used for the study [61]. In the study, the improved LQR control system, LQR systems with optimal values determined using GA, and situations without a control system were compared [61]. In this study, the control system called improved LQR was created using CNN and GA together [61]. Vibrations from wind, cars, subway, and construction were used for vibration data [61]. It was seen that the LQR control system improved by using CNN, and GA gave better performance against normal LQR against different systems and LQR systems with optimized parameters [61].

In the study of Cao and Xue [62], AMD's performance was tried to be improved by using the CNN algorithm [62]. For this, CNN was used to estimate the characteristic change of the vibration. First of all, the system's equation of motion was determined, and the equation of motion was converted into the state-space equation [62]. An electromagnetic force linear actuator was determined for the active control [62]. The optimal feedback control law, which includes CNN algorithm, was determined [62]. After the control law was determined, a numerical study was carried out [62]. In the study, it was evaluated both in the frequency domain and in the time domain. The system's displacement, velocity, and acceleration values were compared with and without AMD [62]. In addition, the conditions before and after the characteristic change of vibration were compared [62]. Finally, as a result of the training using the CNN algorithm, the system's displacement, velocity, and acceleration values were compared [62]. It has been seen that the displacement, velocity, and acceleration values created by using AMD have decreased thanks to the optimal feedback control law developed using the CNN algorithm [62].

5. METHODOLOGY

This section gives detailed information about the methodology used in the thesis.

5.1 Comparison of analytical solution and numerical solution

The first study in the thesis compares the numerical solution method and the analytical solution method determined as a benchmark. The reason for this is to obtain results that are very close to the desired result with numerical solution methods in cases where the analytical solution is insufficient. In order to compare the numerical solution with the analytical solution, the equation of motion of a system is solved. It is assumed that the offshore system used for the first study has a single degree of freedom, and the mass is lumped. In this section the equation of motion used in line with these assumptions is shown in Equation 5.1.

$$m\ddot{q} + c\dot{q} + kq = F(t) \tag{5.1}$$

It is also accepted that the external force acting on the structure is the sinusoidal force. In this way, the mathematical representation of harmonic responses becomes easier. Sinusoidal wave force is shown in Equation 5.2.

$$F(t) = F_0 \sin(\omega_f t) \tag{5.2}$$

$F(t)$ shows the sinusoidal wave force, F_0 is the amplitude of the force, ω_f is the frequency of the force, and t is the time.

The equations used for the analytical solution were obtained from the study of Hibbeler [1]. The ode45 function in the MATLAB programming language is used for the numerical solution. The values of the parameters to be used to compare the analytical and numerical solutions are shown in Table 5.1.

Parameter	Value
m	0.01 t
c	0.01 kNs/m
c_c	0.06 kNs/m
k	0.1 kN/m
F_0	0.005 kN
T	10 s
ω_p	0.6283 Hz
T_{max}	100 s
x_0	2 m
v_0	-1 m/s

Table 5.1 : The values of the parameters used to compare the analytical solution with the numerical solution.

In addition, a study showing the distribution of the Magnification Factor (MF) value according to the ratio of forced frequency and natural frequency has also been carried out [1]. The MF is shown in Equation 5.3 [1].

$$MF = \frac{X^{'}}{F_0/k} \tag{5.3}$$

The expression $X^{'}$ indicates the amplitude steady-state vibrations, while F_0/k indicates static deflection. Finally, the displacement and velocity values obtained by the numerical solution method were examined both in the time domain and in the frequency domain using the Fast Fourier Transform (FFT) algorithm.

5.2 Calculation of wave forces

This section explains wave forces and the equations used to calculate wave forces. Contrary to the use of sinusoidal waves in theoretical studies, it has been accepted that water waves do not show sinusoidal behavior in nature. For this reason, more realistic methods are needed to calculate the wave force. Morison et al. [63] developed an equation to calculate the wave force acting on the cylinder. The Morison equation is shown in Equation 5.4.

$$dF = \frac{1}{2} C_D \rho A u |u| + C_M \rho V \frac{Du}{Dt} \tag{5.4}$$

Here, C_D is the drag coefficient, C_M is the lift coefficient, ρ is the fluid density, A shows the area perpendicular to the flow, u is the horizontal velocity, V shows volume of the body, $\frac{Du}{Dt}$ shows the derivative of the horizontal velocity with respect to time. Equation 5.4 gives the total multichromatic Morison wave force acting at a unit elevation. By integrating the expression, the total wave force can be calculated [64].

$$F = \int_{-h}^{\eta} dF \tag{5.5}$$

However, certain assumptions must be made in order to integrate the expression [64]. First, the variable C_D and C_M coefficients can be considered as constant [64]. The integration provides a certain approximation when using linear wave theory and concentrating on local acceleration terms [64]. For a monochromatic wave the calculation of Morison force gives in Equation 5.6.

$$F = C_D n E_\omega \cos\left(k_\omega x_1 - \omega t\right) \left|\cos\left(k_\omega x_1 - \omega t\right)\right| + C_M \pi D E \frac{D}{H} \tanh k_\omega h \sin\left(k_\omega x_1 - \omega t\right) \tag{5.6}$$

where x_1 is the location of the pile, E_ω is the wave energy per unit surface area, n is the ratio of group velocity, D is the diameter of the pile, H is the wave height, k_ω represents the wave number. By using Equation 5.6 the monochromatic Morison wave force can be calculated. The values of C_D and C_M were determined by referring to the values given in the study of Dean and Dalrymple [64].

5.3 Vibration control of structure against monochromatic Morison wave loading

After comparing the numerical solution method with the analytical solution method, vibration control in the structure under monochromatic Morison force and the feedback control method applied using deep learning are explained in this section. In order to do this, the equation of motion and assumptions used in the previous section are used again. However, to obtain more realistic results, the parameters used for the equation of motion in the first part are considered close to reality. The parameters used in this section are shown in Table 5.2.

Parameter	Value
m	0.15 t
c	0.50 kNs/m
k	2.50 kN/m
g	9.81 m/s^2
C_M	2
C_D	1
H	1 m
h	10 m
ρ	1.02 t/m^3
D	1 m
n	1
T	15 s
x_1	0 m
x_0	2 m
v_0	-1 m/s

Table 5.2 : Parameters used to analyze structure under monochromatic Morison force.

Unlike the first part, the wave loading is calculated as a monochromatic Morison force which is shown in Equation 5.6. After the forecast with LSTM algorithm, which is explained in the next section, Root Mean Square Error (RMSE) was used to check the accuracy of the forecasted and the observed value in Equation 5.7.

$$RMSE = \sqrt{\frac{1}{n}\sum_{i=1}^{n} {e_i}^2} \tag{5.7}$$

where e is error. In addition, the corresponding values of the spectral amplitudes of the observed monochromatic Morison wave force in the frequency domain were compared with the corresponding values of the spectral amplitudes of the forecasted monochromatic Morison wave force in the frequency domain. In this way, it was possible to compare the forecasted and observed values in the frequency domain.
Finally, monochromatic Morison wave force and displacement control were performed using the feedback control strategy as mentioned before.

5.4 Vibration control of structure against multichromatic Morison wave loading

In this section, the vibration control study against multichromatic Morison wave loading is explained.

5.4.1 Construction of the initial wave field

The characteristics of each of the water waves in nature are different. Since they are random in their direction and frequency, their representation in the time domain is complex [2]. However, the corresponding value of the energy of the waves in the frequency domain can be determined. In this way, the wave spectrum was used to express the water waves more clearly. Thanks to the wave spectrum, more complex and realistic wave fields can be obtained than the sinusoidal waves. In that study, the Bretschneider-Mitsuyasu frequency spectrum, one of the studies done by Bretschneider [65], and Mitsuyasu [66], was used to create a realistic wave field. In the study of Bayındır performed in 2009, the calculations made for the construction of the 2D wave field were also used [67]. The Bretschneider-Mitsuyasu frequency spectrum is shown in Equation 5.8.

$$S(f) = 0.257 H_{1/3}^2 T_{1/3}^{-4} f^{-5} \exp[-1.03(T_{1/3} f)^{-4}] \tag{5.8}$$

The expression $S(f)$ denotes wave spectrum $H_{1/3}$ denotes significant wave height, $T_{1/3}$ denotes significant wave period, and f denotes frequency. After obtaining the frequency spectrum, the frequency spectrum was converted to angular frequency spectrum using Equation 5.9 and Equation 5.10.

$$S(f)\frac{df}{d\omega} = S(\omega) \tag{5.9}$$

$$\frac{df}{d\omega} = \frac{1}{2\pi} \tag{5.10}$$

where ω is the angular frequency, and $S(\omega)$ is the angular frequency spectrum. Using Equation 5.11, the angular frequency spectrum is converted to the wavenumber spectrum.

$$S(\omega)\frac{d\omega}{dk_\omega} = S_k(k_\omega) \tag{5.11}$$

k_ω is wavenumber, and $S_{\mathrm{k}}(k_\omega)$ is wavenumber spectrum. Thanks to the dispersion relation showing the relationship between the wavenumber and the angular frequency, the angular frequency spectrum is converted into the wavenumber spectrum. The dispersion relationship is shown in Equation 5.12.

$$\omega^2 = g k_\omega \tanh(k_\omega h) \tag{5.12}$$

h is the water depth, and g is the gravitational acceleration. The $\frac{d\omega}{dk_\omega}$ expression in Equation 5.11 equals the group velocity C_g. The group velocity is shown in Equation 5.13.

$$\frac{d\omega}{dk_\omega} = C_g = \frac{1}{2}\left(1 + \frac{2k_\omega h}{\sinh(2k_\omega h)}\right)\frac{\omega}{k}_{\omega} \tag{5.13}$$

The multiplication of the Equation 5.9 and Equation 5.13, the expression S_k, the wavenumber spectrum, is obtained.

Considering the energy equality, the nodal amplitude values corresponding to each dk_ω can be calculated using Equation 5.14.

$$\frac{1}{2}a_r^2 = S_k(k_r)\, dk_\omega \tag{5.14}$$

where $r = 0,1,2,3,4,\ldots\ldots,N/2$, a_r is nodal amplitude, $dk_\omega = \frac{2\pi}{L}$, L refers to periodic domain length, and $k_r = r dk_\omega$. The number N is selected to be the power of 2. The value of N is chosen as the power of 2. Because the power of 2 must be selected in order to perform the FFT efficiently. Then, the obtained amplitude values were equalized to be symmetrical according to the $N/2$ value in Equation 5.15.

$$a_s = a_{N-s} \tag{5.15}$$

In Equation 5.15, $s = \frac{N}{2}+1, \frac{N}{2}+2, \frac{N}{2}+3, \frac{N}{2}+4, \ldots\ldots N-1$. After the symmetry relationship is shown in Equation 5.15, a phase was added to the system to ensure randomness. This phase, called the symmetrically distributed random phase (θ_j),

for $j = -\frac{N}{2}+1, -\frac{N}{2}+2, -\frac{N}{2}+3 \ldots\ldots \frac{N}{2}$ takes values in the range of $[0, 2\pi]$. After providing the phase to ensure randomness, the complex amplitudes were calculated.

The first complex amplitude (B_j) is calculated using Equation 5.14, Equation 5.15, and (θ_j). The first complex amplitude is shown in Equation 5.16.

$$B_j = \frac{a_j \exp\left(i\Theta_j\right)}{2} \tag{5.16}$$

where $i = \sqrt{-1}$. After obtaining B_j using Equation 5.16, the second complex amplitude (C_j) is calculated by using Equation 5.17.

$$C_j = -\frac{ig}{\omega_j}\frac{a_j}{2}\exp\left(i\Theta_j\right) \tag{5.17}$$

Then the initial water surface elevation (η_p) can be calculated by using B_j. The calculation of η_p is shown in Equation 5.18.

$$\eta_p = \sum_{j=-N/2+1}^{N/2} B_j \exp\left(ik_j x_p\right) \tag{5.18}$$

$x_p = pdx$, $p = 0, 1, 2, 3, \ldots\ldots\ldots, N/2$, $dx = \frac{L}{N}$. After calculating the initial water surface elevation, the initial velocity potential was calculated similarly to the same approach. The initial velocity potential can be calculated using C_j. The calculation of the initial velocity potential is shown in Equation 5.19.

$$\phi_p^s = \sum_{j=-N/2+1}^{N/2} C_j \exp\left(ik_j x_p\right) \tag{5.19}$$

The initial water surface elevation and initial velocity potential are obtained using complex amplitudes and inverse FFT given by Equation 5.18 and Equation 5.19.

5.4.2 Temporal dynamics of 2D linear water wave

Once the initial water surface value and velocity potential are calculated, the water surface elevation and velocity potential in the time series can be calculated using

kinematic and dynamic boundary conditions. The kinematic and dynamic boundary conditions are shown in Equation 5.20 and Equation 5.21.

$$\eta_t + \nabla_h \phi^s . \nabla_h \eta - (1 + \nabla_h \eta . \nabla_h \eta) \phi_z(\vec{x}, \eta, t) = 0 \tag{5.20}$$

$$\phi_t^s + g\eta + \frac{1}{2} \nabla_h \phi^s . \nabla_h \phi^s - \frac{1}{2}(1 + \nabla_h \eta . \nabla_h \eta) \phi_z^2(\vec{x}, \eta, t) = -\frac{P_a}{\rho} \tag{5.21}$$

P_a indicates atmospheric pressure, and ∇_h parameter indicates horizontal gradient, ρ shows the density of the fluid. In this calculation, the flow is assumed to be incompressible, inviscid, and irrotational.

In order to simulate two-dimensional linear water waves, the Equation 5.20 and Equation 5.21 are linearized. The equations obtained after the linearization process are shown in Equations 5.22 and Equation 5.23 [67].

$$\eta_t - \phi_t^s = 0 \tag{5.22}$$

$$\phi_t^s + g\eta = 0 \tag{5.23}$$

A two-dimensional linear water wave model can be obtained by using the solution of Equation 5.22 and Equation 5.23 in the temporal domain. Two-dimensional linear wave simulation is obtained from solving Equation 5.22 and Equation 5.23 with the fourth-order Runge-Kutta method. After solving according to the fourth-order Runge-Kutta method, time-series values of velocity potential and water surface elevation values are obtained. Using the velocity potential, both the horizontal and vertical velocity values at the midpoint of the wavefield could be calculated.

5.4.3 Mechanical properties of the structure

In the last part of our study, the vibration control of the structure against the multichromatic Morison wave force is explained. For theoretical studies, it is seen that water waves are expressed as sinusoidal. However, although the water waves in nature are not sinusoidal, it has been observed that they are extremely difficult and complex

structures to express physically. For this, to create a realistic system, water waves must be expressed in the closest possible way to reality. In addition, the realistic selection of the structure will increase the accuracy of the results obtained. For this reason, Draugen platform in the Norwegian sea was used. Figure 5.1 shows the structure used for our study. Unlike the Draugen platform, it is assumed that the leg does not narrow starting from the ground, and the diameter continues as a constant from the ground to the deck. In addition, as in the previous sections, it is assumed that the system has a single degree of freedom, and the mass of the structure is considered lumped.

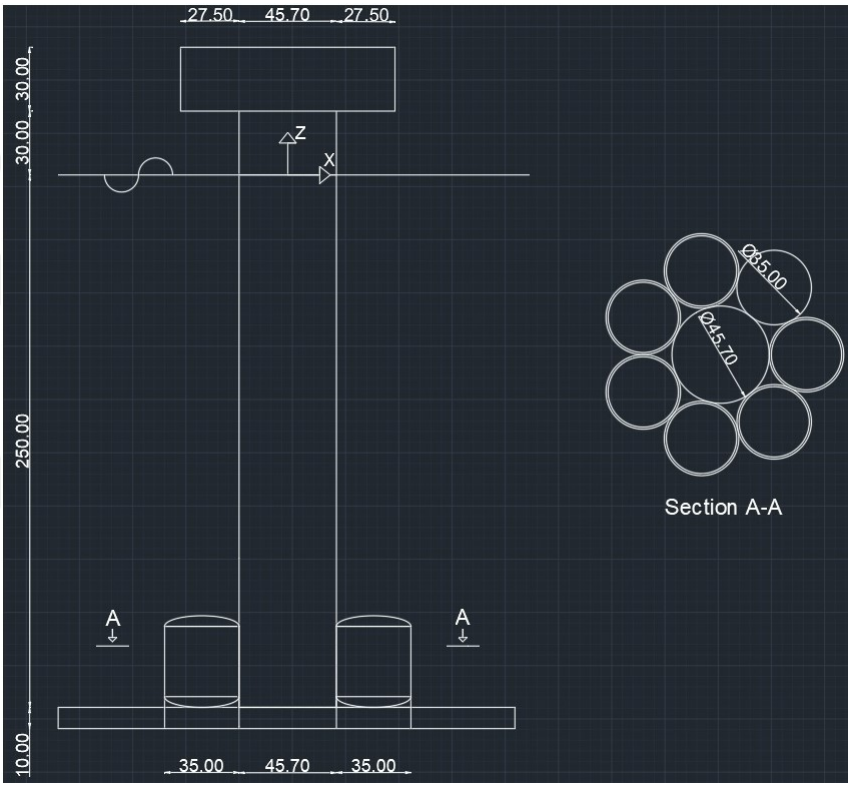

Figure 5.1 : Draugen Platform [68].

After modeling the structure to be used, it is necessary to determine the structure's mechanical properties. For this, the system's mass, stiffness, and damping capacity must be determined.

First of all, to calculate the mass of the structure, it is necessary to know the amount of concrete used in the structure and the properties of the concrete. In addition, the mass of the materials used in the building other than concrete should be known. For this, the values that Alm et al. performed in 1995 used in their studies were used [68]. In addition, [69] was also used for the features of the platform. However, in line with

the information given, the necessary information for the type of concrete used in the structure could not be obtained. So, a search has been done for values that will be important for future calculations. According to Abolitz et al. [70], it was stated that the type of concrete to be used should have a minimum 28-day cylinder compressive strength of at least 35 MPa. However, exact data on the density of concrete could not be obtained. As seen in TS500, the compressive strength of C35/45 concrete is 35 MPa [71]. For this reason, the E value was determined by taking the C35/45 concrete as a reference. The value of E is selected as 33000 MPa [71]. However, in the study of Noguchi and Nemati, since the units of the compressive strength and modulus of elasticity are kgf/cm^2, the unit weight value was calculated by converting the units of the compressive strength and modulus of elasticity from MPa to kgf/cm^2. Equation 5.24 was used in order to obtain the unit weight value [72].

$$E = 2.1 \times 10^5 (\gamma_{conc}/2.3)^{1.5} (f_c/200)^{1/2} \tag{5.24}$$

where E represents the modulus of elasticity, f_c represents the compressive strength, and γ_{conc} represents the unit weight of concrete. The result of the calculation is approximately $\gamma_{conc} \approx 2.60$ t/m^3. Since the unit weight was used as t/m^3 in the study of Noguchi and Nemati, it was used as t/m^3 in this study as well [72].

After determining the unit weight of the concrete, the mass of the structure was calculated according to Equation 5.25.

$$m_{total} = (\gamma_{conc} \times V_{conc}) + m_{mtm} + m_{reinforcement} + m_{cable} \tag{5.25}$$

where m_{total} represents the total mass of the structure, V_{conc} represents the volume of the concrete in the structure, m_{mtm} represents the max topside mass, $m_{reinforcement}$ represents the mass of reinforcement and m_{cable} represents the mass of cables. The result of the calculation is $m_{total} \approx 270680$ tonnes. After calculating the mass of the system, the stiffness coefficient was calculated. Equation 5.26 is used to calculate the stiffness of the structure [73].

$$k = \frac{EA_s}{L} = \frac{33000000 \times 1640.30}{290} = 186654396\text{kN/m} \tag{5.26}$$

where A_s represents the axial area of the structure, L represents the length of the structure. The result of the calculation is approximately $k \approx 186654396$ kN/m. In order to calculate the k value in Equation 5.26, the unit of the E value was converted from MPa to kN/m^2. Another critical parameter for the structure is to determine the damping coefficient of the structure. For this reason, the critical damping of the structure is used to determine the damping coefficient of the structure. The critical damping c_c value of the structure was calculated by using the total mass and stiffness values. Equation 5.27 was used to calculate the critical damping value.

$$c_c = 2m\sqrt{\frac{k}{m}} \tag{5.27}$$

After obtaining the critical damping, it is assumed that the damping coefficient of the structure is equal to 10 percent of the critical damping coefficient.

The result of the calculation is approximately $c \approx 1421599$ kNs/m. After determining the total mass, stiffness, and damping coefficient values of the structure, the equation of motion used in the following sections is specified in Equation 5.28.

$$m\ddot{q} + c\dot{q} + kq = F(t) \tag{5.28}$$

The values of the parameters used for the structure are given in Table 5.3. Finally, multichromatic Morison wave force and displacement control were performed using the feedback control strategy as mentioned before.

5.5 Wave force forecast using LSTM

This section mentions the forecast approaches of monochromatic Morison wave forces and multichromatic Morison wave forces. The parameters and approaches used for the two different studies are the same. The parameters used for forecasting are shown in Table 5.4.

Two different approaches were used for the forecasting process. These approaches are

no updated forecasting and updated forecasting. The first approach is the no updated

Parameter	Value
m_{total}	270680 t
c	1421599 kNs/m
k	186654396 kN/m
E	33000 MPa
g	9.81 m/s^2
D	45.70 m
$\gamma_{concrete}$	2.60 t/m^3
ρ	1.02 t/m^3
A	1640.30 m^2
L	290 m
h	250 m
c_c	14215990 kNs/m
m_{cables}	1500 t
m_{mtm}	27800 t
V_{conc}	86300 m^3
$m_{reinforcement}$	17000 t
C_M	2
C_D	1
$H_{1/3}$	2 m
$T_{1/3}$	10 s
x_0	0.5 m
v_0	-0.2 m/s

Table 5.3 : Parameters used to analyze structure under multichromatic Morison force.

Parameter	Value
Number of hidden layer	200
Number of responses	1
Number of features	1
Maximum epoch	250
Learn rate drop factor	0.2
Verbose	0
Gradient Threshold	1
Initial Learn Rate	0.005
Learn Rate Drop Period	125

Table 5.4 : The values of the parameters used for the prediction.

forecast approach. According to the no updated forecast approach, the LSTM is trained using only values between $[0-45]$ s to forecast the Morison force time series. After the training process is over, the values after the 45th second are forecasted with the values forecasted in the previous time steps.

The second approach is the updated forecast approach. According to the updated forecast approach, the LSTM algorithm is trained using values in the range of $[0-45]$ s. Then, to forecast the monochromatic Morison force and multichromatic Morison force in the t, the values observed in the previous time steps were used together with the values in $[0-45]$ s.

6. RESULTS AND DISCUSSIONS

6.1 Simulated Results for the Mitigation of Offshore Platform Vibrations

This section shows the results of three different studies mentioned earlier. Moreover, the results obtained and what needs to be done to achieve better results are discussed.

6.1.1 The results of analytical solution and numerical solution

First of all, the accuracy of the numerical solution should be verified by comparing it to the analytical solution used as the benchmark problem. In order to make this comparison, the equation of motion of a system with the single degree of freedom was solved analytically and numerically. The same parameters were used for two different solutions. The results of the analytical and numerical solution of the system are shown in Figure 6.1.

As shown in Figure 6.1, the displacement-time graph is obtained as a result of the analytical and numerical solution of the system. The time interval of the solution was chosen in the range of $[0-100]$ s. The initial position of the mass in the system was chosen as $x_0 = 2$ m, and the initial velocity of the mass in the system was chosen as $v_0 = -1$ m/s. The time step value was determined as $dt = 0.1$ s. As seen in Figure 6.1, the c value, which is the damping coefficient of the system, is smaller than the critical damping value c_c of the system, so the system is underdamped. The external force is the sinusoidal force. The study shows that the analytical solution determined as a benchmark and the numerical solution used in the following parts of the study give approximately the same results. In this way, it is accepted that the numerical solution gives the correct result.

In Figure 6.2, the (MF) values of different c/c_c values according to the ratio of the force-frequency and the natural frequency of the system are shown. While the range selected for MF values is $[0-10]$, the range selected for ω_0/ω_n is $[0-5]$ Hz, ζ

represents the c/c_c. Due to the decrease ζ, the MF increases. Especially at the point where $\zeta = 0$ and $\omega_0/\omega_n = 1$, it is seen that the MF value blows. This situation is called resonance.

In Figure 6.1, displacement is evaluated in the time domain. However, better representation of complex signals can be achieved by evaluating them in the frequency domain. For this, spectral analysis was used. The values of the displacement spectral amplitudes in the frequency domain are also shown in Figure 6.3. Figure 6.3 consists of two different graphs. The upper graph shows the relationship between displacement and time, while the lower graph shows the corresponding values of the displacement spectral amplitude in the frequency domain. FFT was used for spectral analysis.

As seen in Figure 6.3, the displacement spectral amplitude peaks at $+0.02$ Hz and -0.02 Hz, where the displacement spectral amplitude value is approximately 0.50. Displacement spectral amplitudes in the positive frequency domain are shown in Figure 6.4. Figure 6.4 consists of two different graphs. While the relationship between displacement and time is shown in the upper graph, the values corresponding to the

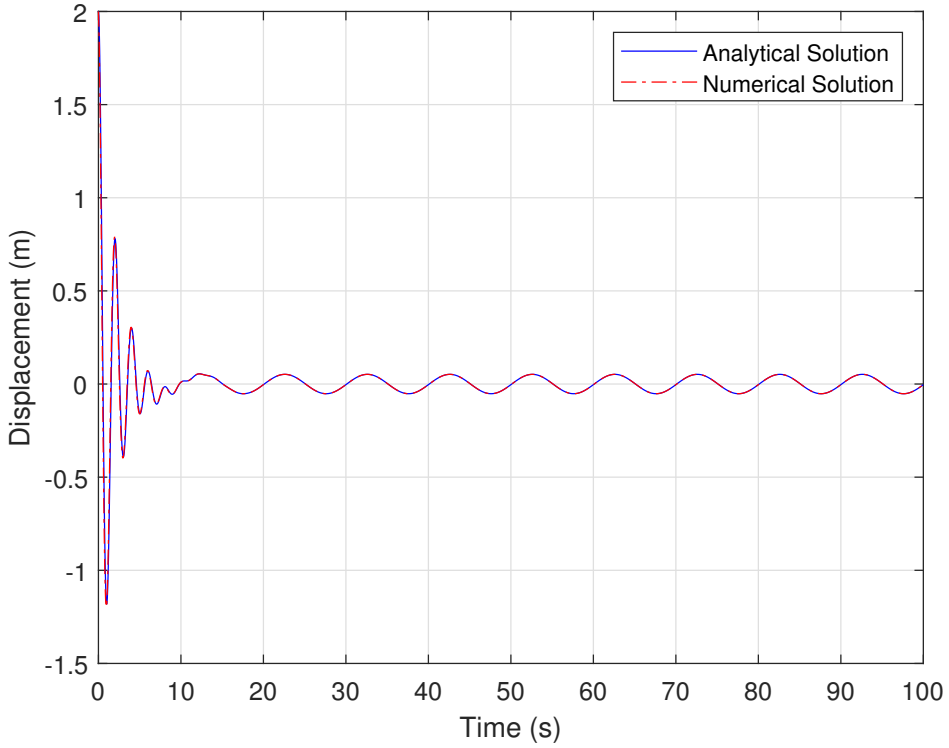

Figure 6.1 : Analytical and numerical solutions.

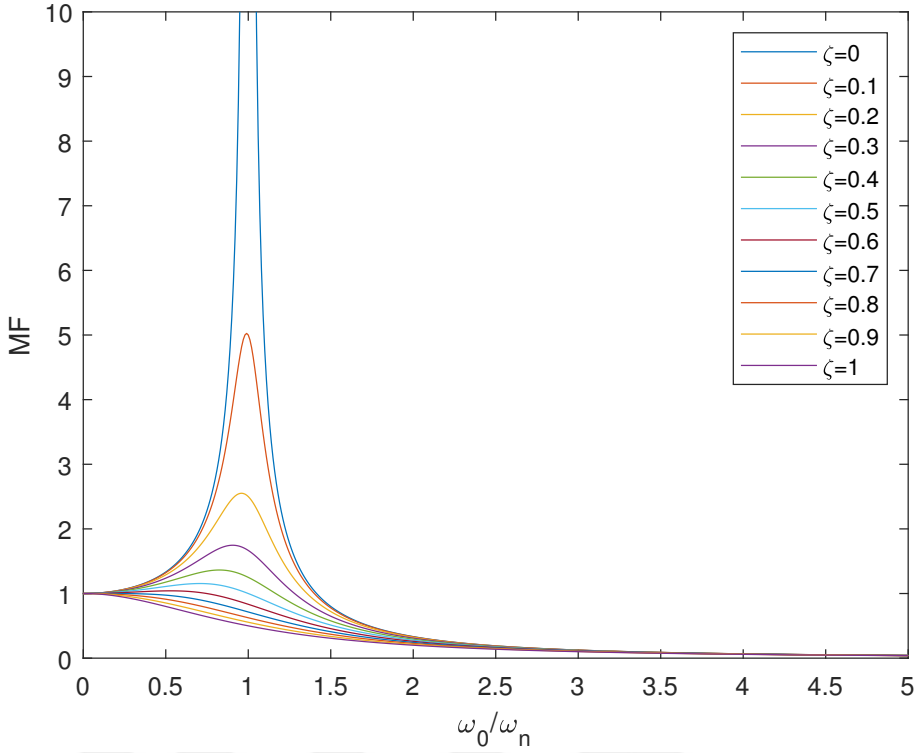

Figure 6.2 : Magnification factor [1].

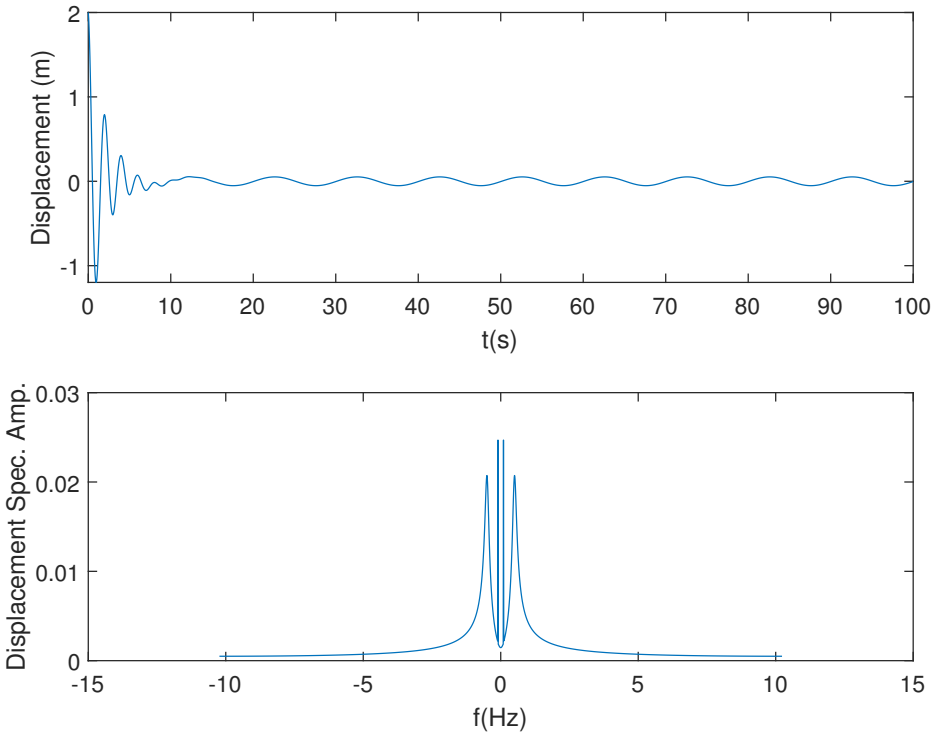

Figure 6.3 : Displacement-time and two-sided displacement spectrum graph.

positive frequency value of the displacement spectral amplitude are shown in the lower graph.

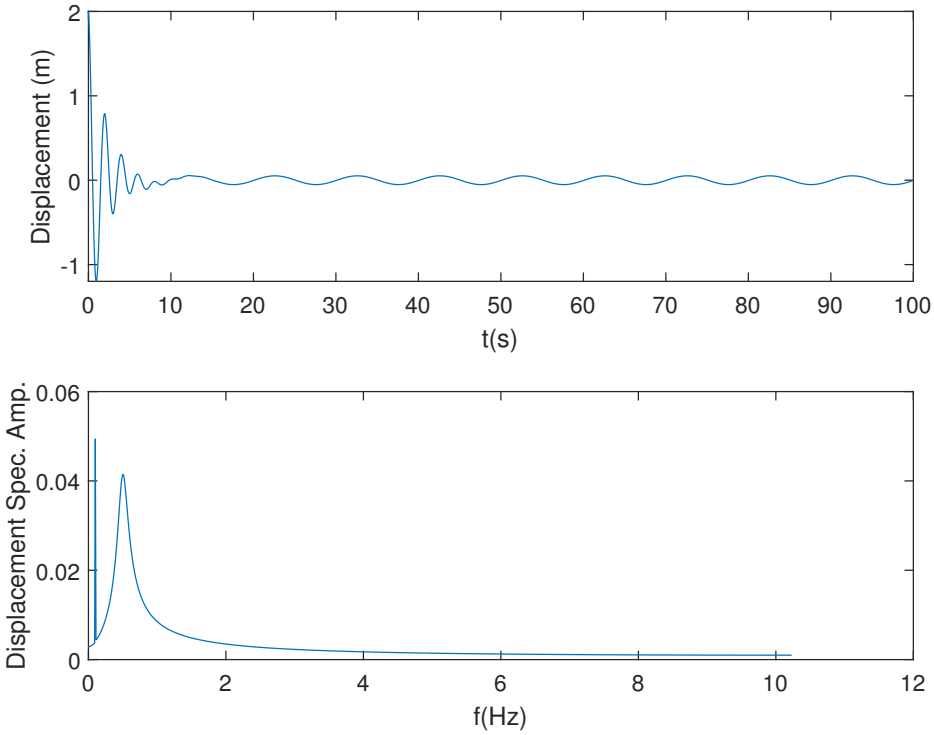

Figure 6.4 : Displacement-time and one-sided displacement spectrum graph.

As seen in Figure 6.4, the displacement spectral amplitude peaks at $+0.04$ Hz, where the spectral amplitude is approximately 0.50. After examining the displacement values, velocity values were examined both in the time domain and in the frequency domain. So, the values of the velocity spectrum are shown in Figure 6.5. In Figure 6.5, the upper graph shows the relationship between velocity and time values, while the lower graph shows the corresponding values of velocity spectral amplitudes in the frequency domain.

As seen in Figure 6.5, the velocity spectral amplitude peaks at $+0.06$ Hz and -0.06 Hz, where the spectral amplitude is approximately 0.49. Likewise, velocity spectral amplitude values corresponding to positive frequency values are shown in Figure 6.6.

As seen in Figure 6.6, the velocity spectral amplitude peaks at 0.12 Hz, where the spectral amplitude is approximately 0.49.

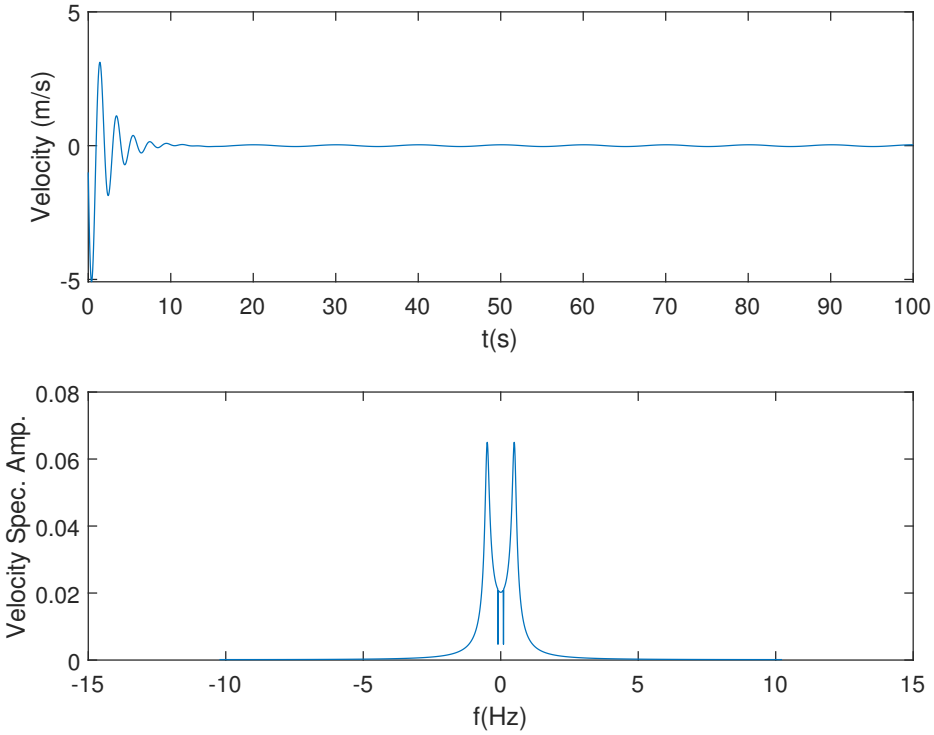

Figure 6.5 : Velocity-time and two-sided velocity spectrum graph.

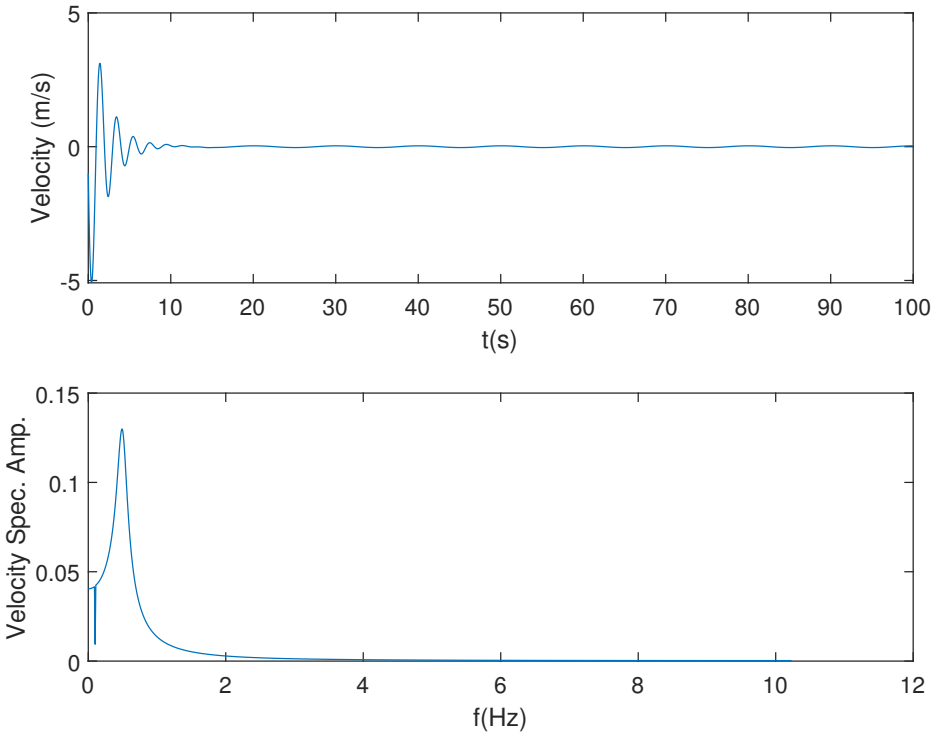

Figure 6.6 : Velocity-time and one-sided velocity spectrum graph.

6.1.2 Vibration control against monochromatic Morison wave loading

The first analysis performed for the second study is to determine the value of the force created by the waves acting on the system. By using the Equation 3.28, monochromatic Morison wave force can be calculated. The relationship between the acting monochromatic Morison force and the time series is shown in Figure 6.7.

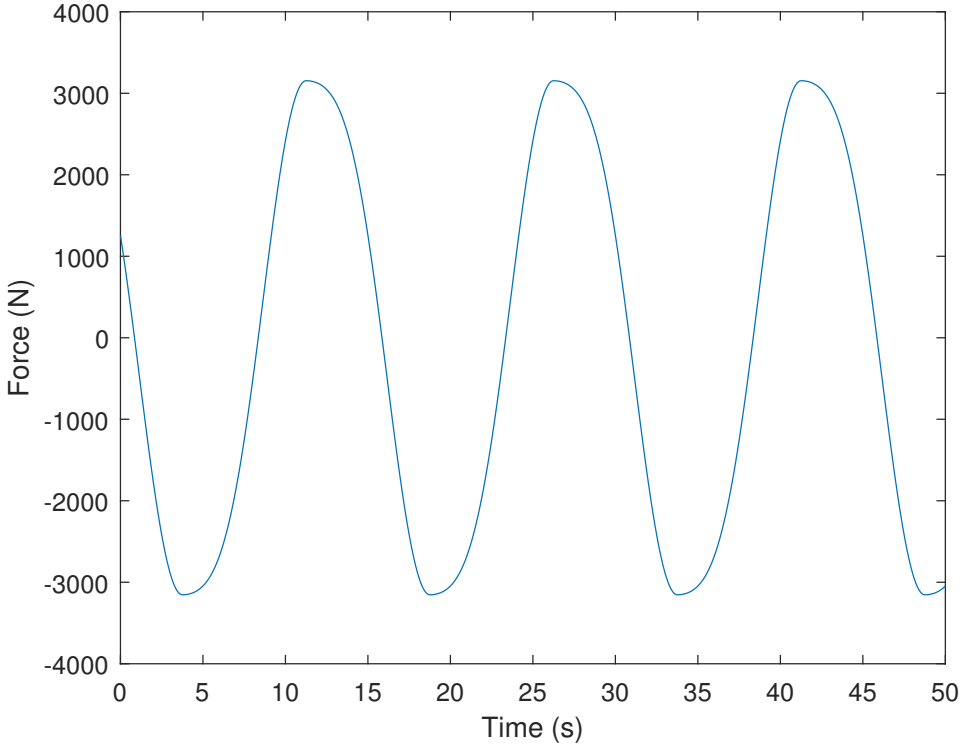

Figure 6.7 : The monochromatic Morison force.

The time interval selected for the system is determined as $[0-50]$ s.

After examining the monochromatic Morison force acting on the system, the force was forecasted in the time series. Two different approaches were used for the forecast, the no-update forecast, and the updated forecast. In both approaches, LSTM architecture is used.

The first approach is the no-update forecast approach. Figure 6.8 shows the results obtained using the no-update forecast approach.

Error analysis results using RMSE are shown in Figure 6.9. Figure 6.9 consists of two graphs. The upper graph shows the observed and forecasted monochromatic Morison

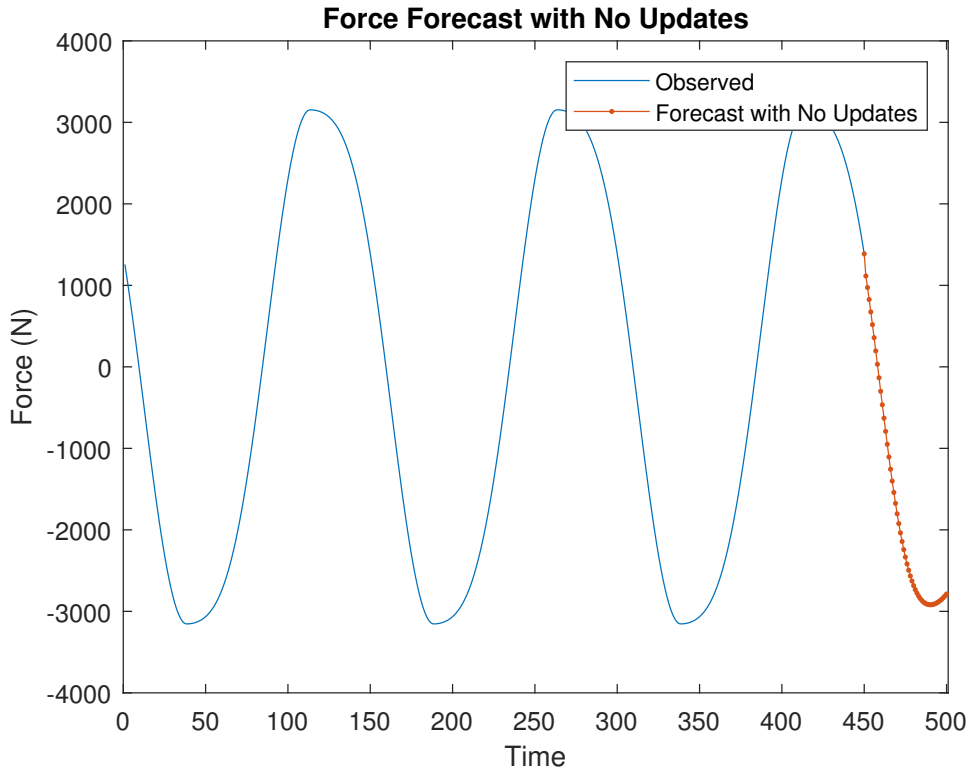

Figure 6.8 : Force forecast with no update.

force. The error analysis made using RMSE is shown in the graph below. As can be seen, when the time step increases, the error value in the forecast increases.

The results of spectral analysis of the observed and forecasted monochromatic Morison force is shown in Figure 6.10.

In the second approach, the updated forecast approach was used. The forecast results obtained using the updated forecast approach are shown in Figure 6.11.

RMSE was used to calculate the accuracy of the values in the updated forecast, likewise the no-update forecast. Error analysis of the updated forecast using RMSE is shown in Figure 6.12.

Figure 6.12 consists of two different graphs. The upper graph shows the observed and updated forecast values of the monochromatic Morison force. Results of the error analysis by using RMSE are shown in the graph below.

As can be seen in Figure 6.9 and Figure 6.12, the error value in the updated forecast approach is lower than the error value of the no-update forecast approach.

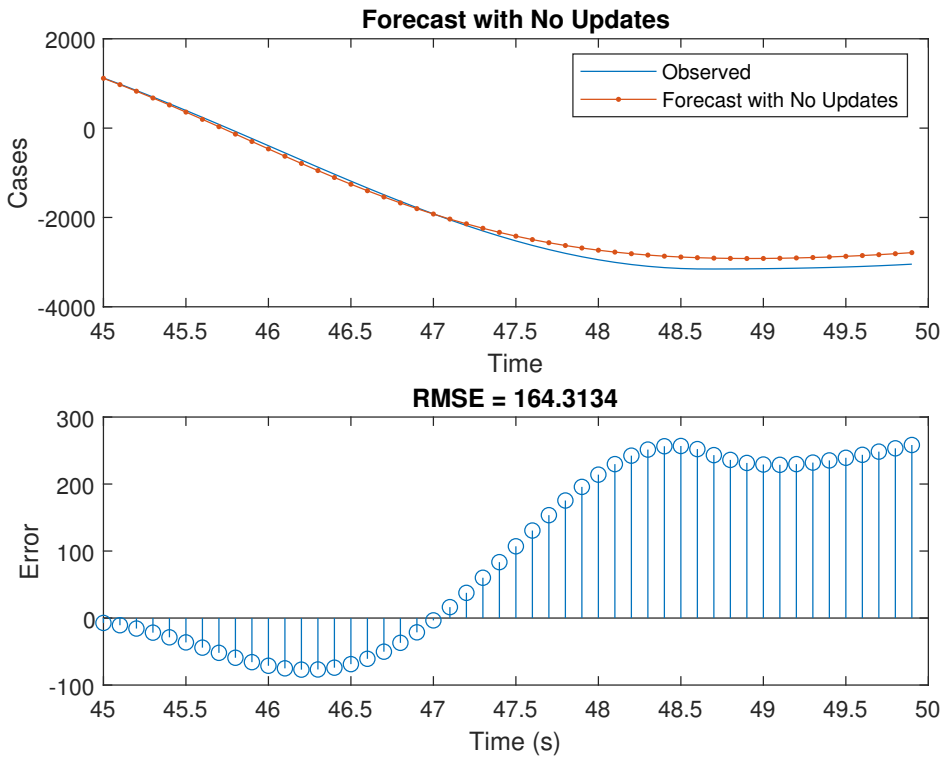

Figure 6.9 : Error analysis for no updated forecast.

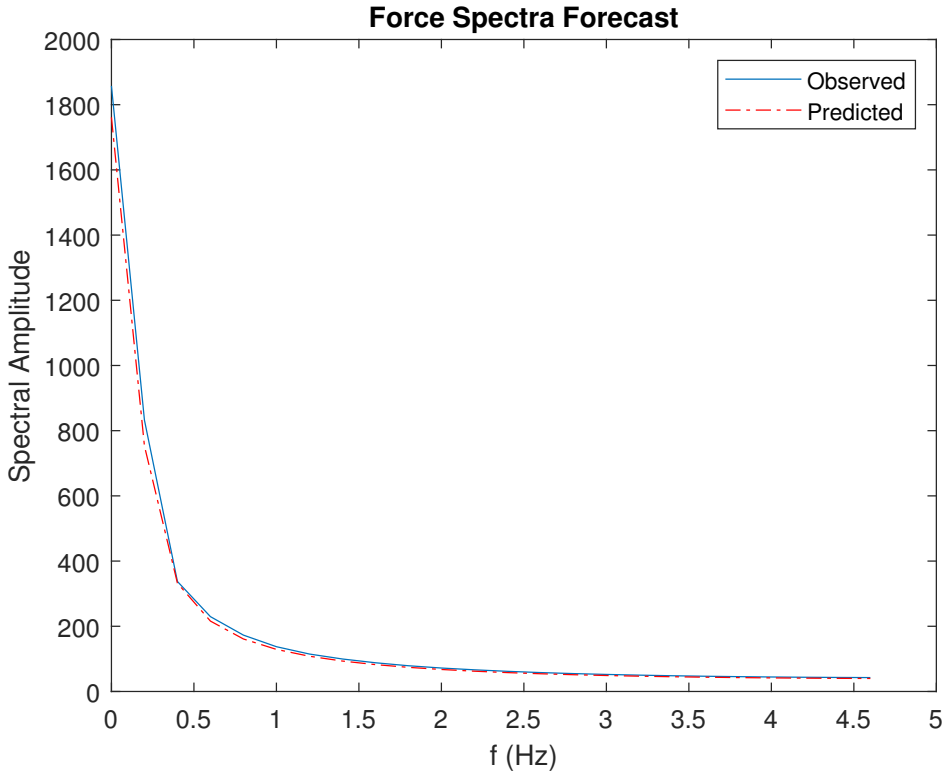

Figure 6.10 : Force spectra forecast with no update forecast.

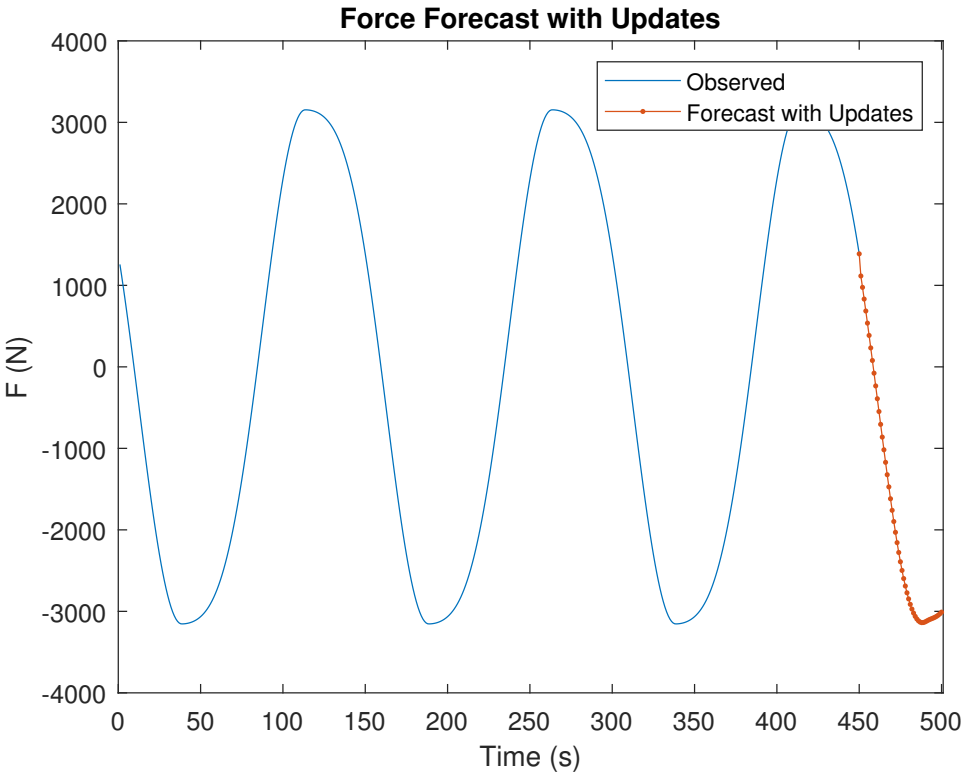

Figure 6.11 : Updated monochromatic Morison force forecast.

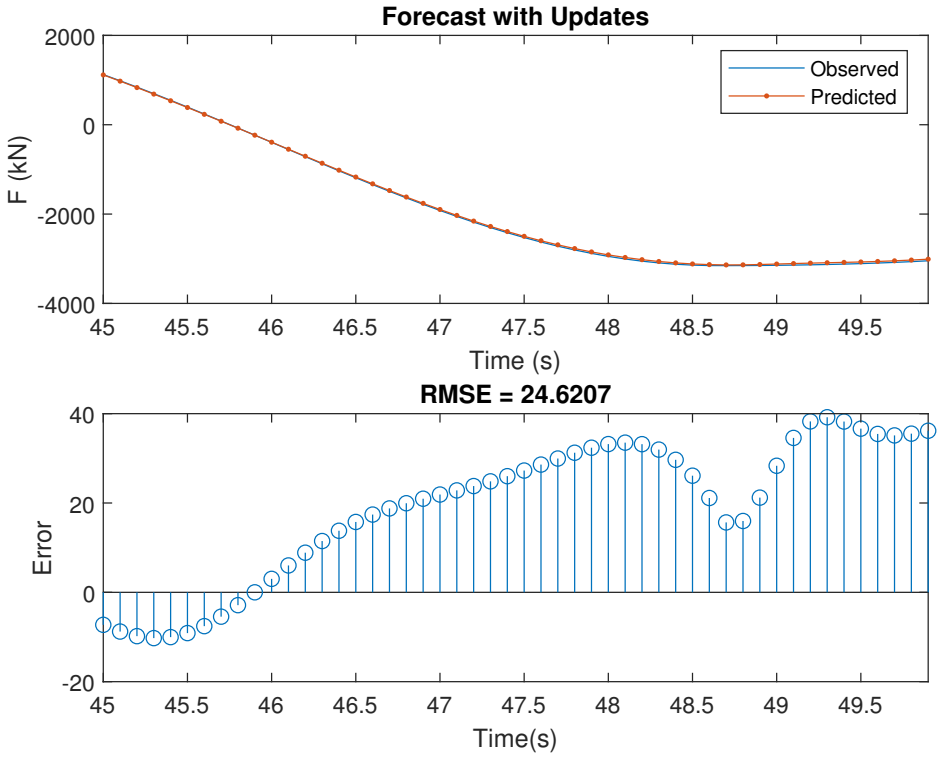

Figure 6.12 : Error analysis for updated forecast.

In the Figure 6.13, the spectrum of the updated forecasted force values and the observed force values are shown.

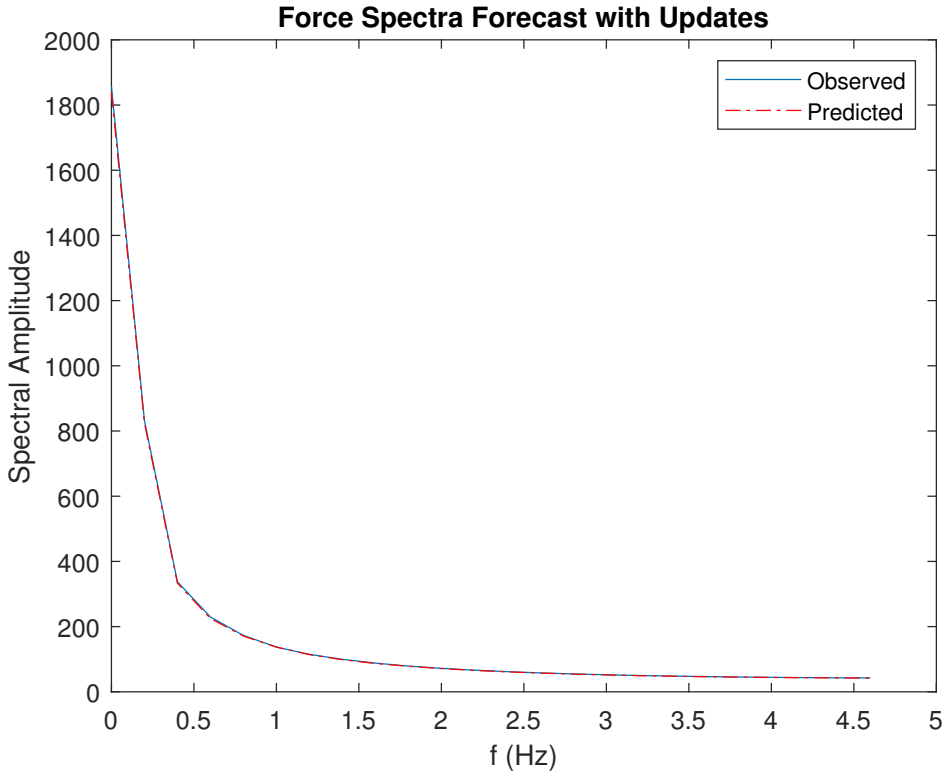

Figure 6.13 : Force spectra forecast with updates.

The force forecast made by the updated forecast approach gives more accurate results. For this reason, an updated forecast approach is used to control the monochromatic Morison force. The force values obtained from the updated forecast approach are called the control force which is shown in Equation 3.29 as $F_D(t)$. The control force $F_D(t)$ in Equation 3.29 is given to the system as feedback in the opposite direction to the wave force, and the force acting on the structure is tried to be controlled. The results are shown in Figure 6.14.

Figure 6.14 consists of two graphs. The upper graph shows the corresponding values of the monochromatic Morison force in the time series. The graph below shows the corresponding values in the time series of the absolute force acting on the structure due to the control force acting in the opposite direction. As seen in Figure 6.14, the control of monochromatic Morison force was achieved after 45 seconds. For this reason, the displacement was also controlled. The displacement results obtained from the decrease in the absolute force acting on the structure are shown in Figure 6.15.

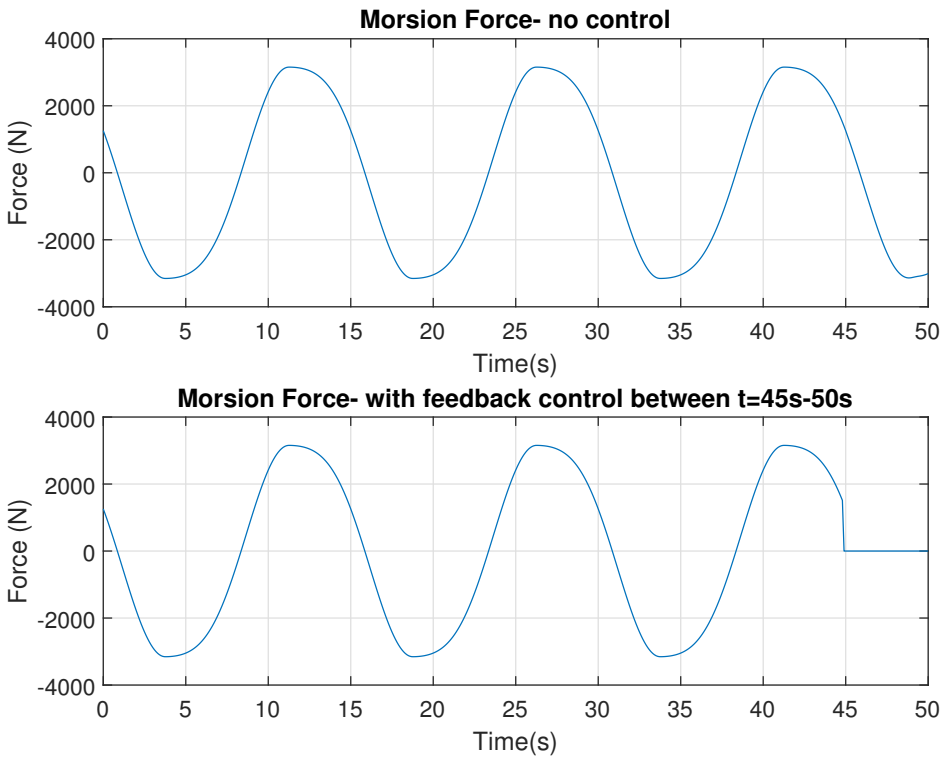

Figure 6.14 : Control of monochromatic Morison force.

In Figure 6.15, consists of two different graphs. The upper graph shows the change in the time series of the displacement caused by the effect of the monochromatic Morison force. The graph below shows the corresponding values in the time series of the absolute force acting on the structure due to the control forces acting on the system. As can be seen from Figure 6.15, the vibration that occurs after the 45th second is mitigated and controlled. In this way, it has been shown that vibration occurring in a structure with a single degree of freedom against monochromatic Morison force can be controlled by using the LSTM algorithm.

6.1.3 Vibration control against multichromatic Morison wave loading

In this section, various changes have been made to obtain more realistic results than previous studies. First of all, as mentioned before, the mechanical properties of the Draugen platform were used to obtain realistic results. Furthermore, a realistic wave field was obtained using the wave spectrum. After creating a realistic wave field, the force value applied to the Draugen platform, theoretically placed in the middle of the wave field, becomes more realistic. The information required for the study has been

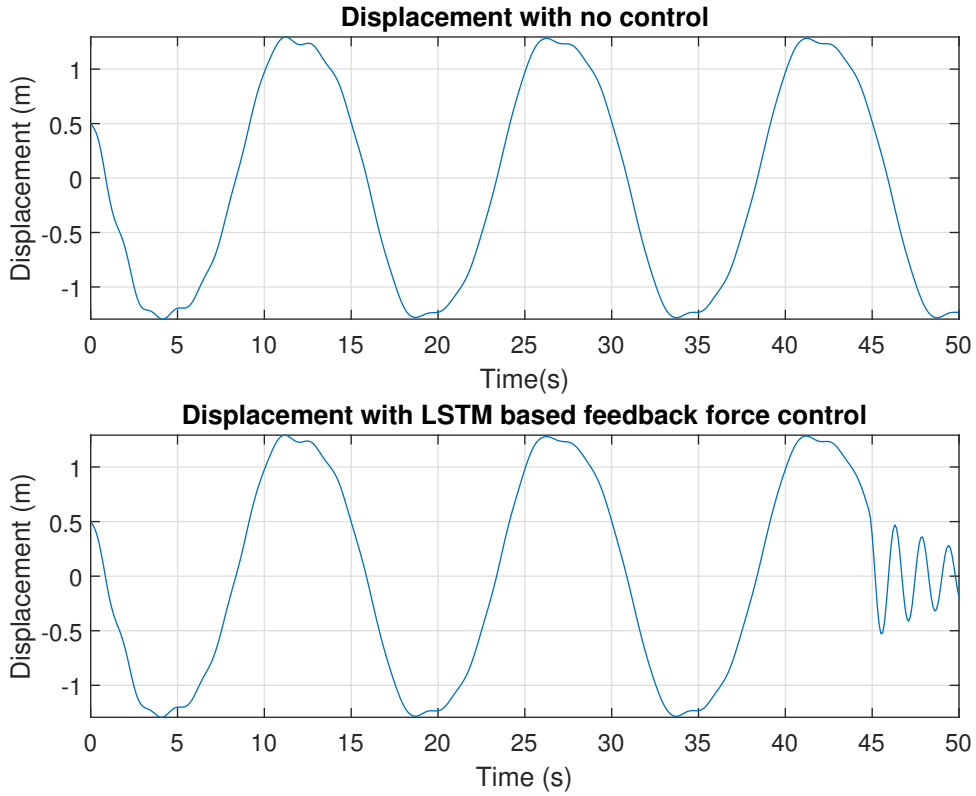

Figure 6.15 : Vibration control against monochromatic Morison force.

summarized in Table 3.2 and Table 3.3. Also, the horizontal velocity and horizontal acceleration values of the point in the middle of the wave field were calculated to calculate multichromatic Morison wave forces. The horizontal velocity and horizontal acceleration at the midpoint of the wave field are shown in Figure 6.16.

After obtaining the horizontal velocity and horizontal acceleration values, Equation 3.26 was used to calculate the multichromatic Morison force acting on the structure. Corresponding values of the multichromatic Morison force in the time series are shown in Figure 6.17.

Once obtaining the multichromatic Morison force values against time, the forecast approach was made using the LSTM algorithm as it was done in the second study. For the forecast process, the LSTM algorithm was trained using multichromatic Morison force values in $[0-45]$ s. Then, with the training of the LSTM algorithm, the values after 45 seconds were forecasted with updated and no updated forecasted approaches. The forecast process is shown in Figure 6.18.

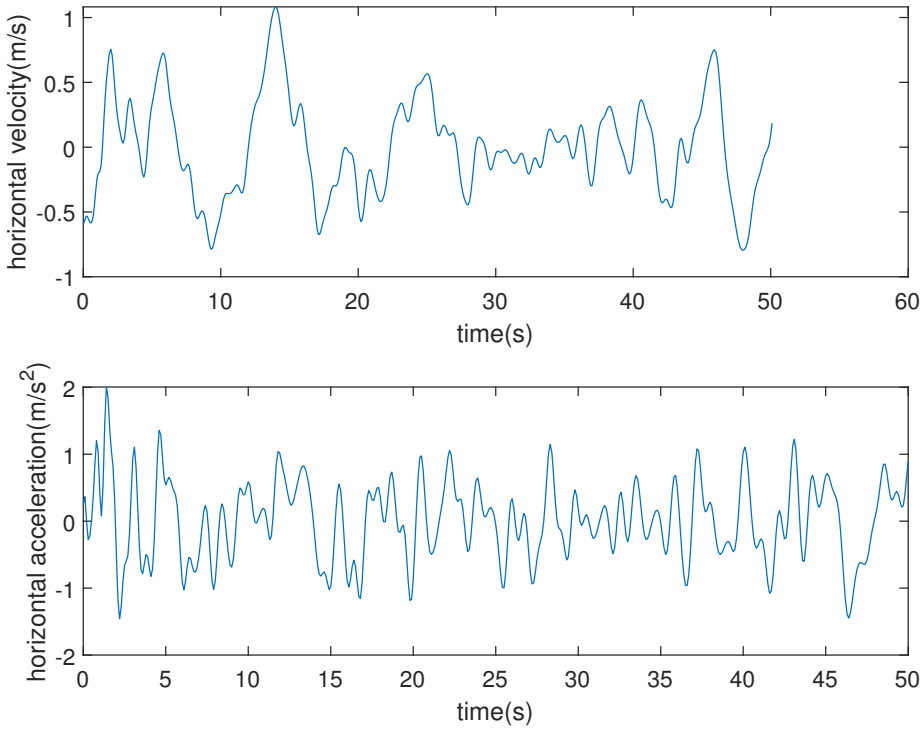

Figure 6.16 : Horizontal velocity and horizontal acceleration time graph.

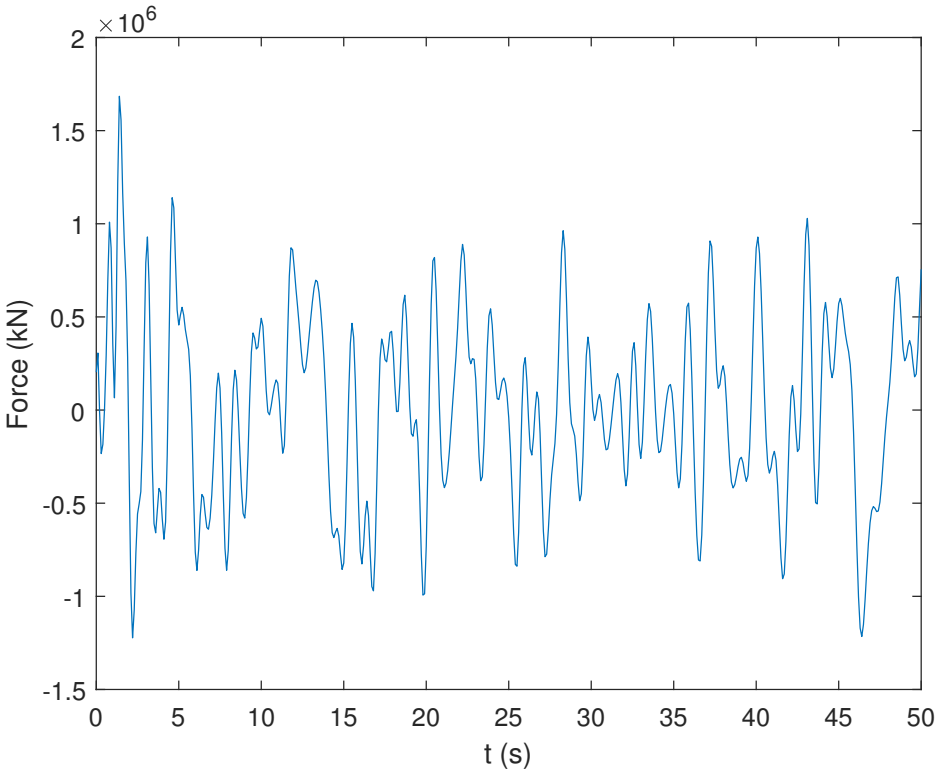

Figure 6.17 : The multichromatic Morison force.

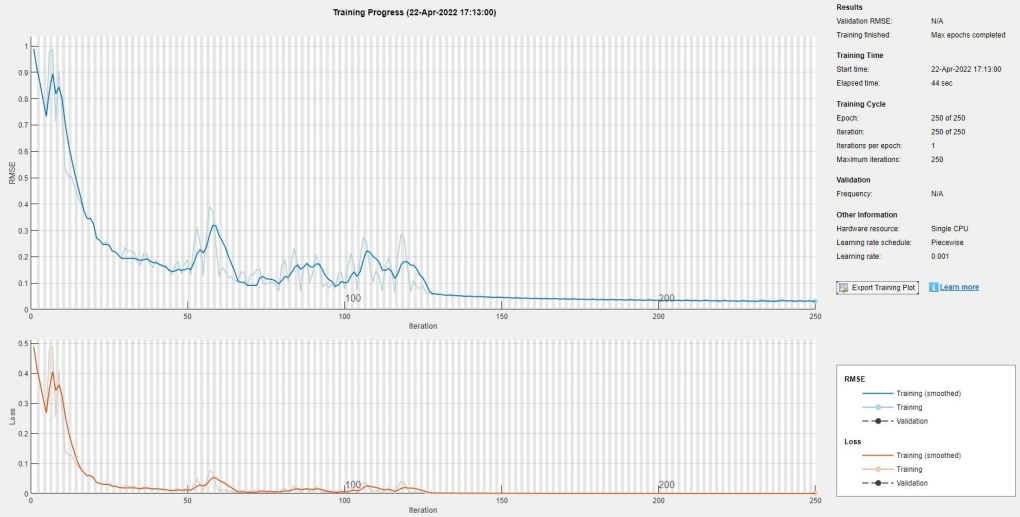

Figure 6.18 : Training progress.

After the training, updated and no-update forecast approaches were made for the multichromatic Morison force. The forecast results of the multichromatic Morison force by using the no-update forecast approach are shown in Figure 6.19.

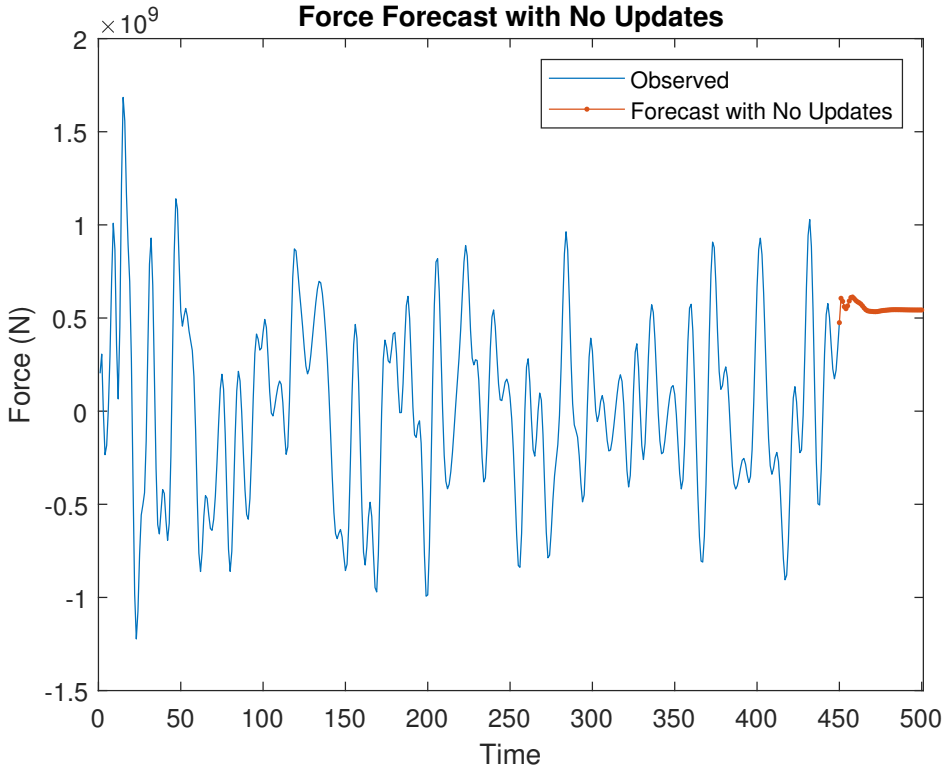

Figure 6.19 : Multichromatic Morison force forecast with no update.

According to the result obtained from Figure 6.19, it has been seen that the forecast made with the no-update approach could not give the desired values. The forecast results obtained by performing the updated approach are shown in Figure 6.20.

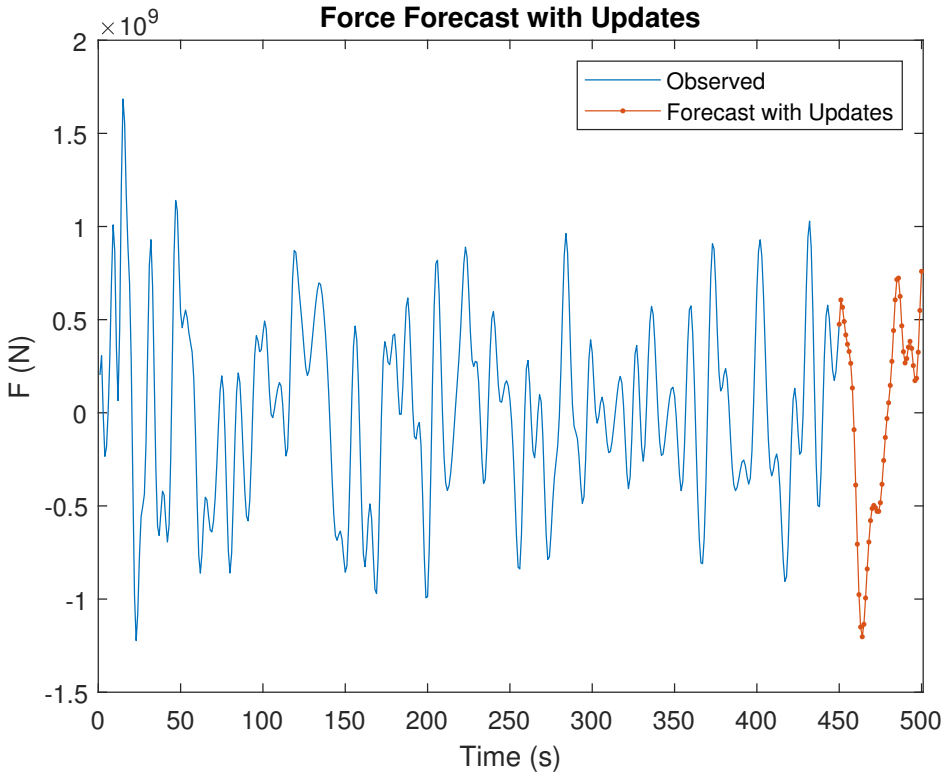

Figure 6.20 : Multichromatic Morison force forecast with updated.

Checking Figures 6.19 and Figure 6.20, the updated forecast approach is more accurate than the no-update forecast approach. RMSE was used to evaluate the performance of the forecasts made. The error analysis results of the values obtained from the forecast of the multichromatic Morison force with no-update approach are shown in Figure 6.21.

The error analysis results of the values obtained from the prediction of the multichromatic Morison force with updated approach are shown in Figure 6.22.

It is seen from the Figure 6.21 and Figure 6.22 that error value is less when forecast was done with updated forecast approach. In Figure 6.23, the observed and forecasted multichromatic Morison force values by using the no updates forecast approach are shown in the corresponding to the frequency domain.

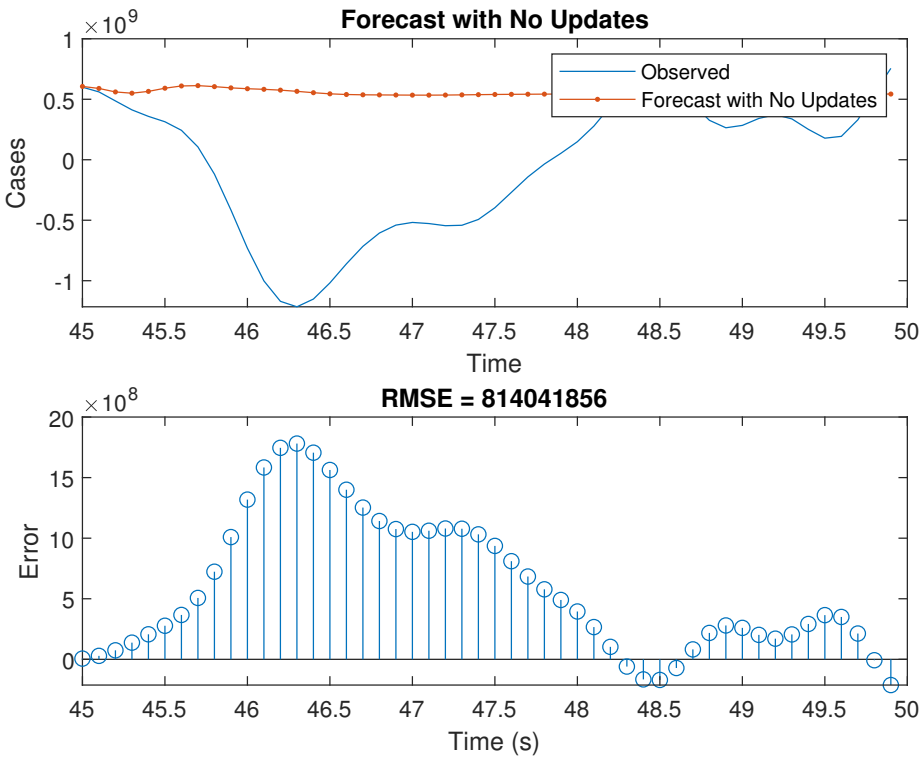

Figure 6.21 : Error analysis for no updated forecast.

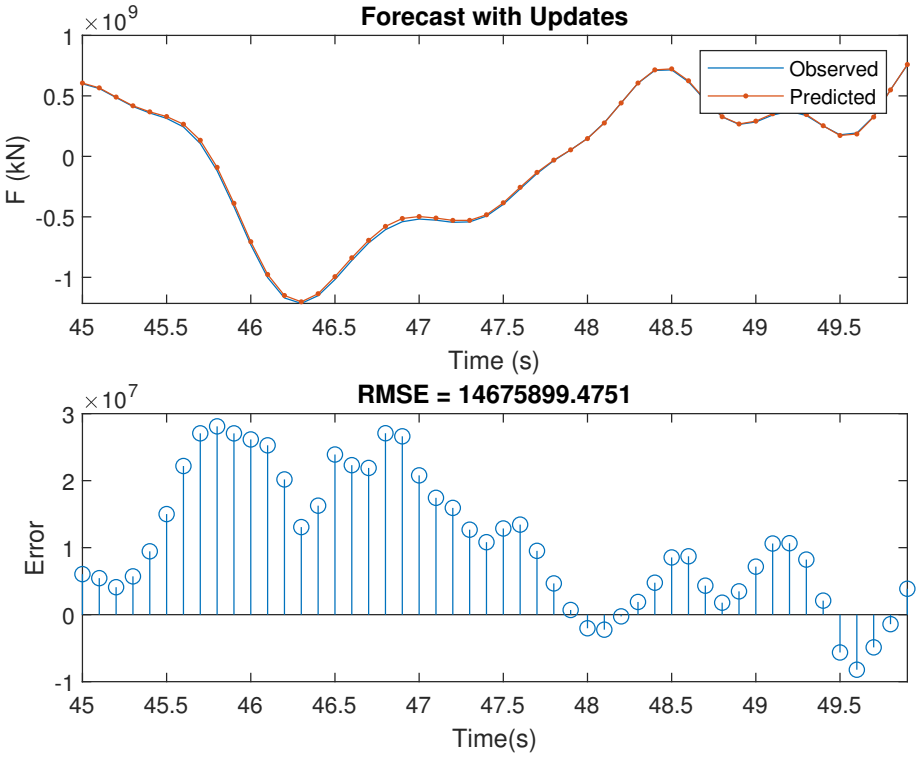

Figure 6.22 : Error analysis for updated forecast.

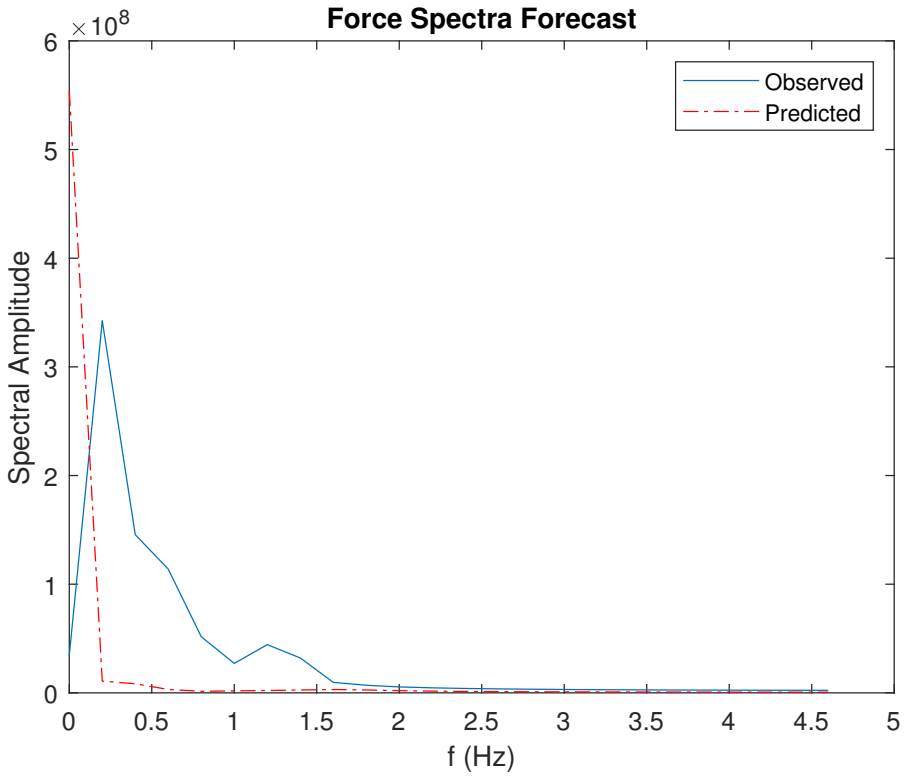

Figure 6.23 : Spectral amplitude-frequency with no updating forecast.

In Figure 6.24, the observed and forecasted multichromatic Morison force values by using the updated forecast approach are shown in the corresponding to the frequency domain. Unlike the forecast with the no-update, it is seen that the forecasted force spectral amplitudes give almost the same results as the observed force spectral amplitudes.

Since the updated forecast gives more accurate results than no-update, it has been decided to use it in force control and vibration control. For this reason, the force values obtained as a result of the forecast the update approach are used as $F_D(t)$ in Equation 3.29. The result obtained as a result of solving Equation 3.29 is shown in Figure 6.25.

Figure 6.25 consists of two graphs. The graph above shows the change in the time series of the multichromatic Morison force acting on the structure. The graph below shows the total force, which is the summation of multichromatic Morison force and control forces acting on the structure in the time series. As can be seen in Figure 6.25, it is seen that the monochromatic Morison force affecting the structure is controlled by

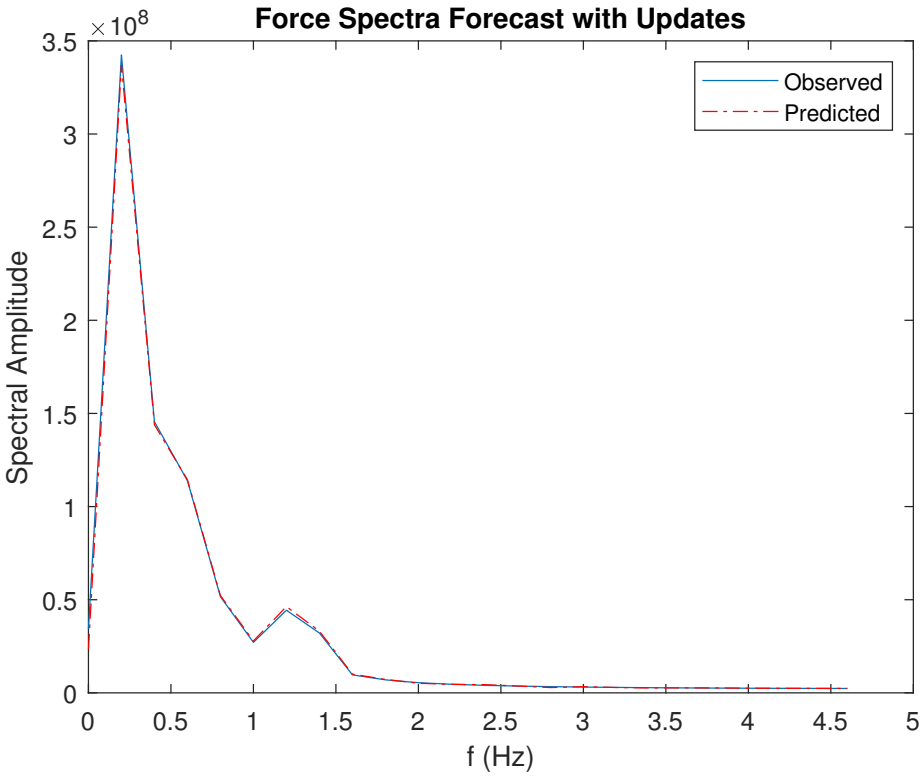

Figure 6.24 : Spectral amplitude-frequency with updating forecast.

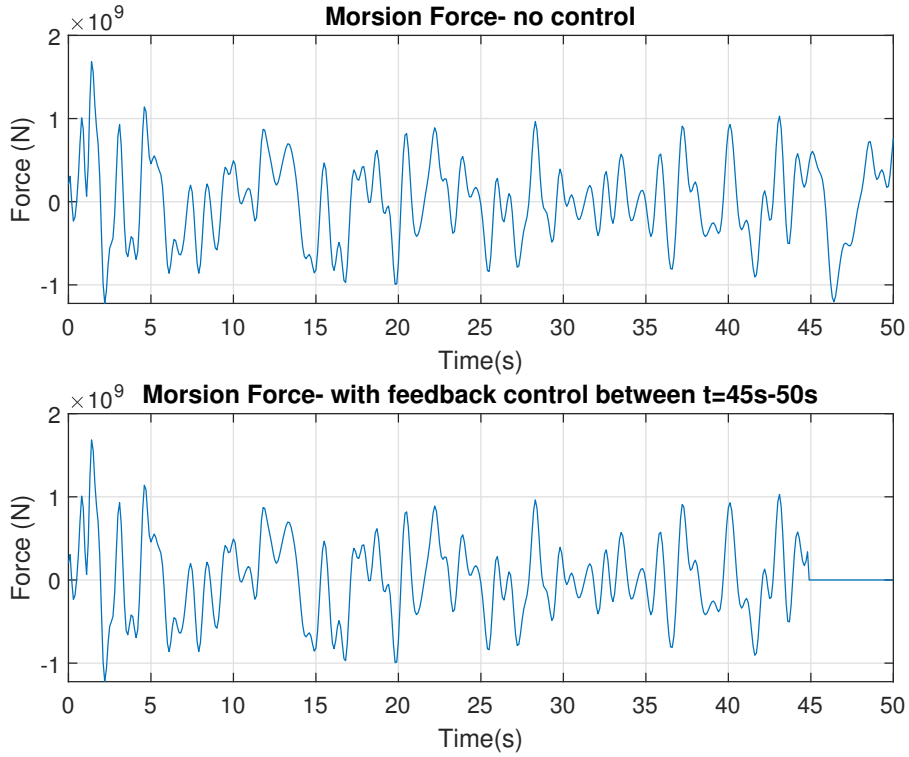

Figure 6.25 : Multichromatic Morison force controlled by feedback method.

giving the forecasted multichromatic Morison wave force as feedback to the system. In addition to controlling the wave force acting on the structure, it aims to control the structure's displacement. For this, the displacement before and after the control force affects the structure was examined. The results are shown in Figure 6.26.

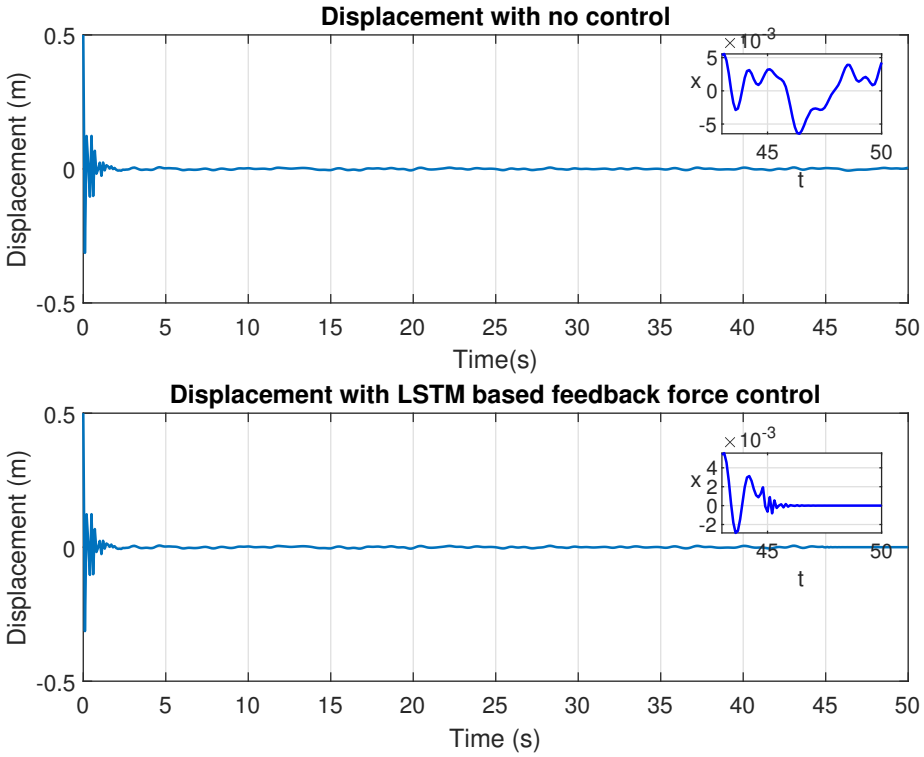

Figure 6.26 : Displacement time values before and after control force is applied.

Figure 6.26 again consists of two graphs. In the graphic above, the displacement of the structures is shown in $[0-50]$ s. The graph below shows the displacement that occurs due to the control force being fed back to the system after the 45th second. In Figure 6.26, it is seen that the displacement of the structure decreases as a result of the multichromatic Morison wave force controlled by the LSTM algorithm. In this way, it is seen that the desired result is achieved.

6.1.4 Comparison of different significant wave heights and significant wave periods

In this section, the effect of different wave height values and different wave period values on displacement is examined. First of all, different significant wave height values were used for comparison. The values of all parameters except the significant

wave height values were taken the same. The results are shown in Figure 6.27 and Figure 6.28.

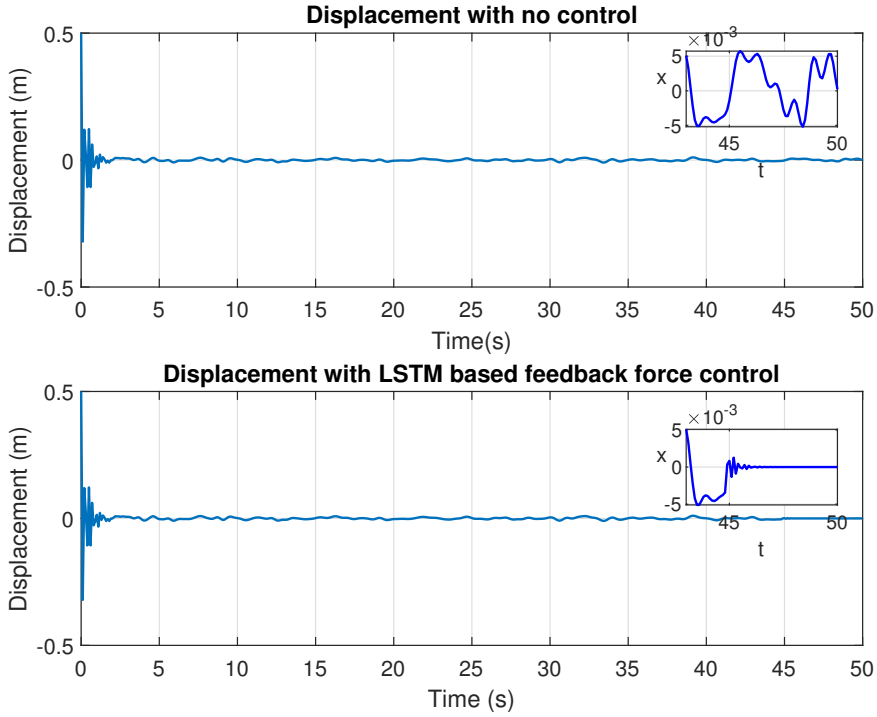

Figure 6.27 : The displacement values obtained for $H_{1/3} = 3$ m and $T_{1/3} = 10$ s.

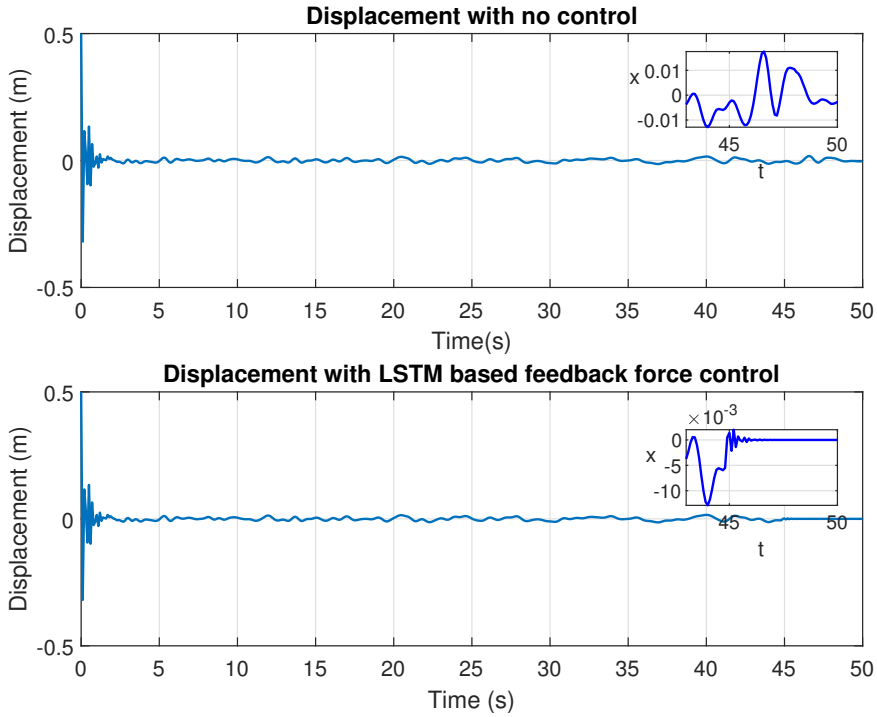

Figure 6.28 : The displacement values obtained for $H_{1/3} = 5$ m and $T_{1/3} = 10$ s.

In Figure 6.27, $H_{1/3}$ is assigned to be 3 meters. In Figure 6.28, $H_{1/3}$ is selected to be 5 meters. The significant wave period of Figure 6.27 and Figure 6.28 are selected to be 10 seconds. After the comparison of significant wave heights, different significant wave periods are compared. The results of the comparison are shown in Figure 6.29 and Figure 6.30.

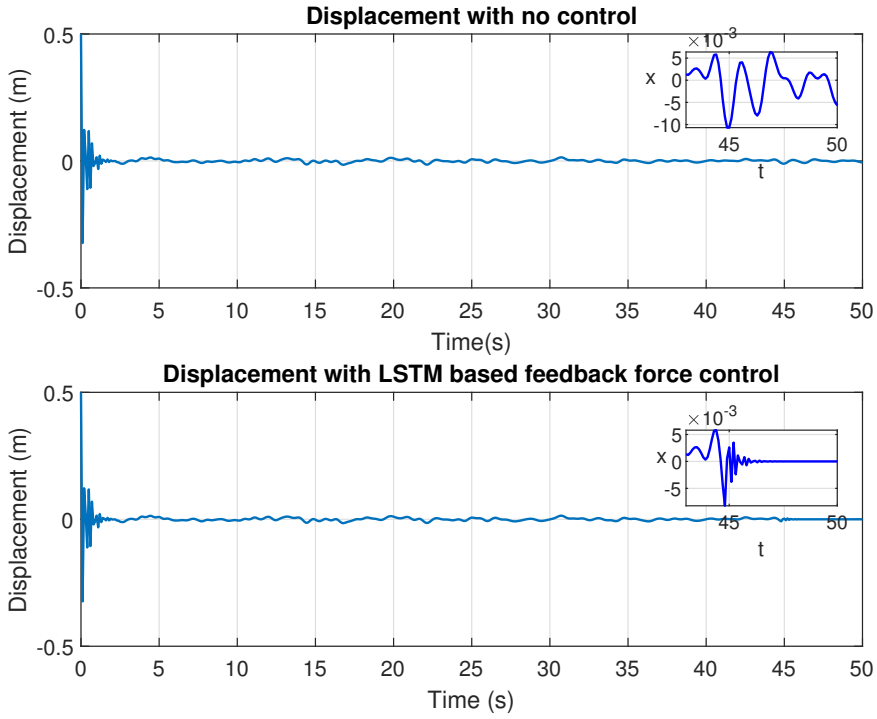

Figure 6.29 : The displacement values obtained for $H_{1/3} = 4$ m and $T_{1/3} = 10$ s.

In Figure 6.29 $T_{1/3}$ is selected as 10 seconds. In Figure 6.30 $T_{1/3}$ is selected as 15 seconds. The significant wave height of Figure 6.29 and Figure 6.30 are selected to be 4 meters.

As can be seen in the comparisons, it is seen that vibration control can be done successfully by using various significant wave height and wave period value. As a result of the studies, it has been seen that vibration control can be done successfully with the feedback provided by the forecast using the LSTM algorithm.

In this study, vibration control was performed using the feedback control strategy. As can be seen in Figure 6.14 and Figure 6.25, it is seen that the total force F_D control forces acting on the structure is 0 as a result of giving feedback to the system. Since the control forces acting on the system are theoretically perfect. As a result, it is seen that the displacement value also decreases. However, the control force to be applied to

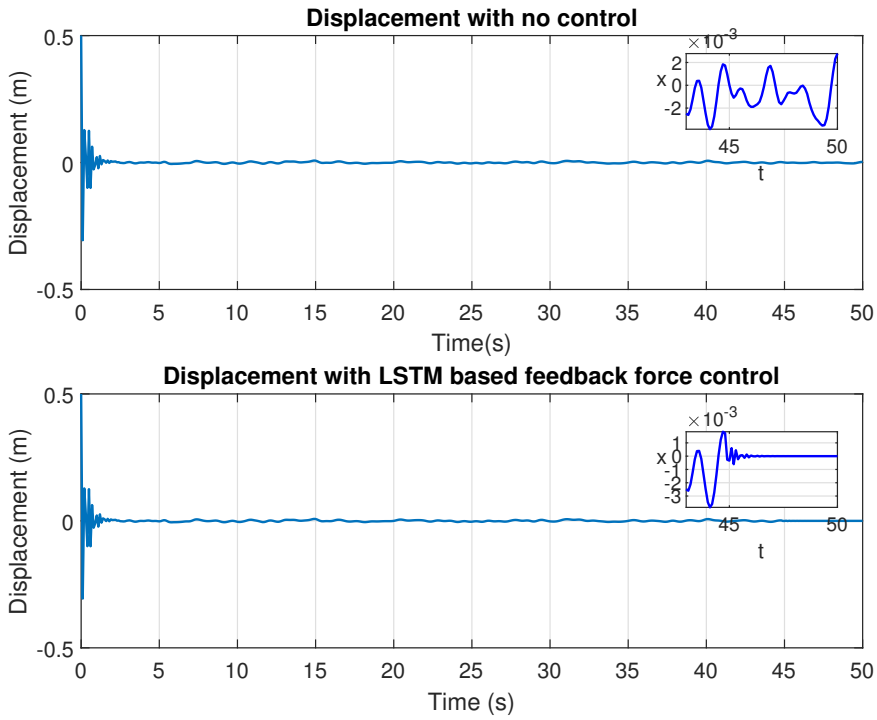

Figure 6.30 : The displacement values obtained for $H_{1/3} = 4$ m and $T_{1/3} = 15$ s.

control the vibration in any system is never perfect. Controlling the vibration occurring in any system can be done proportionally. However, the efficiency of the previously mentioned control systems can be increased by using the LSTM algorithm. In this way, better results can be obtained.

7. CONCLUSIONS

In this study, it is aimed to reduce the displacement by controlling the vibration in the structure by using the LSTM algorithm, which is one of the deep learning algorithms against the forces acting on the existing offshore platform. First of all, the analytical equations were compared with the numerical solution method created using the MATLAB programming language. The accuracy of the numerical solution was demonstrated in the comparison where the analytical solution was accepted as a benchmark. The obtained displacement and velocity values are discussed both in the frequency and time domains. In the second part, the LSTM algorithm is used to control the vibration resulting from the monochromatic wave force acting on a sample structure with a single degree of freedom. The wave force acting on the structure was calculated by the Morison equation. The first 45 seconds of the obtained 50 seconds of monochromatic Morison wave force were used for training in the LSTM algorithm. The forecast results, error analysis, and spectral amplitude values of the updated and no updated forecast approaches using LSTM were compared with the observed values. As a result of the study, since the updated forecast approach gives more accurate results than the no updated forecast approach, the updated forecast process is used for monochromatic Morison wave force control and vibration control. Using the updated forecast approach, the forecasted wave force is given as a control force. After the predicted force was determined as the control force, it was given feedback to the system. The total force value affecting the structure and the resulting vibration values are shown. In the last part, a realistic wave field is created to investigate vibration control realistically. The frequency spectrum was used to create the wave field. As a result of the procedures, the initial water surface elevation and initial velocity potential ??were obtained. After obtaining the initial water surface elevation and velocity potential, 50-second values were obtained using Runge-Kutta time integration. The horizontal velocity and horizontal acceleration values of the point where the structure was placed in the middle of the wave field were located theoretically. Multichromic

Morrison wave force was calculated using the Morrison equation. Then, using the first 45 seconds of the 50-second multichromatic Morison force value, the values after the 45th second were forecasted with and without updates. As a result of the comparison made similar to the study in the second study, the updated forecast approach was used because the updated forecast approach obtained more accurate results than the no updated forecast approach. The wave forces forecasted by the updated forecast approach were determined as the control force. Wave forces determined as control forces are given as feedback to the system. Finally, the absolute force value affecting the system and the change in vibration values were examined. Obtained results are discussed.

In order to obtain more realistic results in future studies, the use of systems where the wave forces acting on the system are nonlinear will allow more realistic results to be obtained. The inclusion of nonlinear wave force and external factors affecting offshore structures such as earthquake load, wind load, and glacial load in the study allows realistic results to be obtained. Vibration control can also be performed using the state variable feedback control strategy mentioned earlier. Finally, using systems with multiple degrees of freedom in the study is also an important factor.

Since the study is theoretical, the control force obtained using the LSTM algorithm is excellent. However, perfect control cannot be achieved by using control forces in the real world. Therefore, the vibration occurring in the system can be controlled proportionally. Vibration control can be done using the control systems mentioned earlier. The efficiency of the systems used can be increased with the LSTM algorithm. The external force acting on the structure can be forecasted by the LSTM algorithm and fed back to the system. In addition, vibration control can be performed by forecasting the displacement and velocity values with the state variable feedback control strategy mentioned earlier.

REFERENCES

[1] **Hibbeler, R.C.** (2010). *Engineering Mechanics: Dynamics*, Pearson Educación.

[2] **Goda, Y.** (2010). *Random Seas and Design of Maritime Structures*, World Scientific Publishing Company.

[3] **Ou, J.**, **Long, X.**, **Li, Q. and Xiao, Y.** (2007). Vibration control of steel jacket offshore platform structures with damping isolation systems, *Engineering Structures*, *29*(7), 1525–1538.

[4] **Patil, K. and Jangid, R.** (2005). Passive control of offshore jacket platforms, *Ocean Engineering*, *32*(16), 1933–1949.

[5] **Chandrasekaran, S.**, **Kumar, D. and Ramanathan, R.** (2013). Dynamic response of tension leg platform with tuned mass dampers, *Journal of Naval Architecture and Marine Engineering*, *10*(2), 149–156.

[6] **Han, Z.**, **Zhao, J.**, **Leung, H.**, **Ma, K.F. and Wang, W.** (2019). A review of deep learning models for time series prediction, *IEEE Sensors Journal*, *21*(6), 7833–7848.

[7] **Gensler, A.**, **Henze, J.**, **Sick, B. and Raabe, N.** (2016). Deep Learning for solar power forecasting—An approach using AutoEncoder and LSTM Neural Networks, *2016 IEEE international conference on systems, man, and cybernetics (SMC)*, IEEE, pp.002858–002865.

[8] **Chimmula, V.K.R. and Zhang, L.** (2020). Time series forecasting of COVID-19 transmission in Canada using LSTM networks, *Chaos, Solitons & Fractals*, *135*, 109864.

[9] **Reddy, D. and Swamidas, A.** (2013). *Essentials of Offshore Structures: Framed and Gravity Platforms*, CRC press.

[10] **Chandrasekaran, S.** (2015). *Dynamic Analysis and Design of Offshore Structures*, Springer.

[11] **Barltrop, N.D. and Adams, A.J.** (1991). *Dynamics of Fixed Marine Structures*, Butterworth-Heinemann.

[12] **Kharade, A. and Kapadiya, S.** (2014). Offshore engineering: an overview of types and loadings on structures, *International Journal of Structural and Civil Engineering Research*, *3*(2), 16–28.

[13] **Hays, D.**, **McSwiggan, M. and Vilain, R.** (1979). Operation of an articulated oil loading column at the Beryl field in the North Sea, *Offshore Technology Conference*, OnePetro.

[14] **Adrezin, R.**, **Bar-Avi, P. and Benaroya, H.** (1996). Dynamic response of compliant offshore structures, *Journal of aerospace engineering*, *9*(4), 114–131.

[15] **Islam, N.**, **Zaheer, M.M. and Ahmed, S.** (2009). Double hinged articulated tower interaction with wind and waves, *Journal of Wind Engineering and Industrial Aerodynamics*, *97*(5-6), 287–297.

[16] **Reza, A. and Sedighi, H.M.** (2015). Nonlinear vertical vibration of tension leg platforms with homotopy analysis method, *Advances in Applied Mathematics and Mechanics*, *7*(3), 357–368.

[17] **Ma, K.T.**, **Luo, Y.**, **Kwan, C.T.T. and Wu, Y.** (2019). *Mooring System Engineering for Offshore Structures*, Gulf Professional Publishing.

[18] **Ng, C.**, **Kurian, V. and Mohamed, M.** (2009). Diffraction method for spar platforms.

[19] **Housner, G.**, **Bergman, L.A.**, **Caughey, T.K.**, **Chassiakos, A.G.**, **Claus, R.O. and Masri, Sami F, .Y.J.T.** (1997). Structural control: past, present, and future, *Journal of engineering mechanics*, *123*(9), 897–971.

[20] **Cheng, F.Y.** (2008). *Smart Structures: Innovative Systems for Seismic Response Control*, CRC press.

[21] **Naeim, F. and Kelly, J.M.** (1999). *Design of Seismic Isolated Structures: From Theory to Practice*, John Wiley & Sons.

[22] **Zhang, B.L.**, **Han, Q.L. and Zhang, X.M.** (2017). Recent advances in vibration control of offshore platforms, *Nonlinear Dynamics*, *89*(2), 755–771.

[23] **Javanmardi, A.**, **Ibrahim, Z.**, **Ghaedi, K.**, **Ghadim, H.B. and Hanif, M.U.** (2020). State-of-the-art review of metallic dampers: testing, development and implementation, *Archives of Computational Methods in Engineering*, *27*(2), 455–478.

[24] **Cimellaro, G.P. and Marasco, S.** (2018). *Introduction to Dynamics of Structures and Earthquake Engineering*, Springer.

[25] **Soong, T. and Spencer Jr, B.** (2002). Supplemental energy dissipation: state-of-the-art and state-of-the-practice, *Engineering structures*, *24*(3), 243–259.

[26] **Soong, T.T. and Costantinou, M.C.** (2014). *Passive and Active Structural Vibration Control in Civil Engineering*, Springer.

[27] **Kandasamy, R.**, **Cui, F.**, **Townsend, N.**, **Foo, C.C.**, **Guo, J.**, **Shenoi, A. and Xiong, Y.** (2016). A review of vibration control methods for marine offshore structures, *Ocean Engineering*, *127*, 279–297.

[28] **Symans, M.D. and Constantinou, M.C.** (1999). Semi-active control systems for seismic protection of structures: a state-of-the-art review, *Engineering structures*, *21*(6), 469–487.

[29] **Hrovat, D.**, **Barak, P. and Rabins, M.** (1983). Semi-active versus passive or active tuned mass dampers for structural control, *Journal of Engineering Mechanics*, *109*(3), 691–705.

[30] **Hao, T.** (2001). Electrorheological fluids, *Advanced Materials*, *13*(24), 1847–1857.

[31] **Vasanth, X.A.**, **Paul, P.S.**, **Lawrance, G. and Varadarajan, A.** (2019). Vibration control techniques during turning process: a review, *Australian Journal of Mechanical Engineering*.

[32] **Carlson, J. and Sproston, J.** (2000). Controllable fluids in 2000-status of ER and MR fluid technology, *7 th International Conference on New Actuator*, pp.126–130.

[33] **Dyke, S. and Spencer, B.** (1997). A comparison of semi-active control strategies for the MR damper, *Proceedings Intelligent Information Systems. IIS'97*, IEEE, pp.580–584.

[34] **Saaed, T.E.**, **Nikolakopoulos, G.**, **Jonasson, J.E. and Hedlund, H.** (2015). A state-of-the-art review of structural control systems, *Journal of Vibration and Control*, *21*(5), 919–937.

[35] **Kavyashree, B.**, **Patil, S. and Rao, V.S.** (2021). Review on vibration control in tall buildings: from the perspective of devices and applications, *International Journal of Dynamics and Control*, *9*(3), 1316–1331.

[36] **Xu, Z.D.**, **Guo, Y.Q.**, **Zhu, J.T. and Xu, F.H.** (2016). *Intelligent Vibration Control in Civil Engineering Structures*, Academic Press.

[37] **Inman, D.J.** (2017). *Vibration with Control*, John Wiley & Sons.

[38] **Caterino, N.** (2015). Semi-active control of a wind turbine via magnetorheological dampers, *Journal of Sound and Vibration*, *345*, 1–17.

[39] **Leng, D.**, **Xiao, H.**, **Sun, L.**, **Liu, G.**, **Wang, X. and Sun, L.** (2019). Study on a magnetorheological elastomer-base device for offshore platform vibration control, *Journal of Intelligent Material Systems and Structures*, *30*(2), 243–255.

[40] **Wang, S.Q. and Li, N.** (2021). Semi-active vibration control for offshore platforms based on LQG method, *Journal of Marine Science and Technology*, *21*(5), 9.

[41] **Gattulli, V. and Ghanem, R.** (1999). Adaptive control of flow-induced oscillations including vortex effects, *International Journal of Non-Linear Mechanics*, *34*(5), 853–868.

[42] **Terro, M.**, **Mahmoud, M. and Abdel-Rohman, M.** (1999). Multi-loop feedback control of offshore steel jacket platforms, *Computers & structures*, *70*(2), 185–202.

[43] **Som, A. and Das, D.** (2018). Seismic vibration control of offshore jacket platforms using decentralized sliding mode algorithm, *Ocean Engineering*, *152*, 377–390.

[44] **Taghikhany, T.** (2013). The effect of semi-active controller in Sirri jacket seismic vibration control, *International Journal of MArine Science and Environment*, *3*(2), 77–84.

[45] **Chollet, F.** (2021). *Deep Learning with Python*, Simon and Schuster.

[46] **LeCun, Y.**, **Bengio, Y. and Hinton, G.** (2015). Deep learning, *nature*, *521*(7553), 436–444.

[47] **Jiao, L. and Zhao, J.** (2019). A survey on the new generation of deep learning in image processing, *IEEE Access*, *7*, 172231–172263.

[48] **Deng, L.**, **Hinton, G. and Kingsbury, B.** (2013). New types of deep neural network learning for speech recognition and related applications: An overview, *2013 IEEE international conference on acoustics, speech and signal processing*, IEEE, pp.8599–8603.

[49] **Kirchgässner, G.**, **Wolters, J. and Hassler, U.** (2012). *Introduction to Modern Time Series Analysis*, Springer Science & Business Media.

[50] **Sezer, O.B.**, **Gudelek, M.U. and Ozbayoglu, A.M.** (2020). Financial time series forecasting with deep learning: A systematic literature review: 2005–2019, *Applied soft computing*, *90*, 106181.

[51] **Şeker, A.**, **Diri, B. and Balık, H.H.** (2017). Derin öğrenme yöntemleri ve uygulamaları hakkında bir inceleme, *Gazi Mühendislik Bilimleri Dergisi (GMBD)*, *3*(3), 47–64.

[52] **Albawi, S.**, **Mohammed, T.A. and Al-Zawi, S.** (2017). Understanding of a convolutional neural network, *2017 international conference on engineering and technology (ICET)*, Ieee, pp.1–6.

[53] **Kizrak, M.A. and Bolat, B.** (2018). Derin öğrenme ile kalabalık analizi üzerine detaylı bir araştırma, *Bilişim Teknolojileri Dergisi*, *11*(3), 263–286.

[54] **Pouyanfar, S.**, **Sadiq, S.**, **Yan, Y.**, **Tian, H.**, **Tao, Y.**, **Reyes, M.P.**, **Shyu, M.L.**, **Chen, S.C. and Iyengar, S.S.** (2018). A survey on deep learning: Algorithms, techniques, and applications, *ACM Computing Surveys (CSUR)*, *51*(5), 1–36.

[55] **Chen, X.W. and Lin, X.** (2014). Big data deep learning: challenges and perspectives, *IEEE access*, *2*, 514–525.

[56] **Shrestha, A. and Mahmood, A.** (2019). Review of deep learning algorithms and architectures, *IEEE access*, *7*, 53040–53065.

[57] **Hochreiter, S. and Schmidhuber, J.** (1997). Long short-term memory, *Neural computation*, *9*(8), 1735–1780.

[58] **Goodfellow, I.**, **Bengio, Y. and Courville, A.** (2016). *Deep Learning*, MIT press.

[59] **Yu, Y.**, **Si, X.**, **Hu, C. and Zhang, J.** (2019). A review of recurrent neural networks: LSTM cells and network architectures, *Neural computation*, *31*(7), 1235–1270.

[60] **Gago, J.J.**, **Vasco, V.**, **Łukawski, B.**, **Pattacini, U.**, **Tikhanoff, V.**, **Victores, J.G. and Balaguer, C.** (2019). Sequence-to-sequence natural language to humanoid robot sign language, *arXiv preprint arXiv:1907.04198*.

[61] **Lu, X.**, **Liao, W.**, **Huang, W.**, **Xu, Y. and Chen, X.** (2021). An improved linear quadratic regulator control method through convolutional neural network–based vibration identification, *Journal of Vibration and Control*, *27*(7-8), 839–853.

[62] **Cao, M. and Xue, S.** Preventing Deterioration of Active Vibration Control Effect Due to Aging Deterioration and Damage based on Deep Learning, *Materials Research Proceedings*, *18*.

[63] **Morison, J.**, **Johnson, J. and Schaaf, S.** (1950). The force exerted by surface waves on piles, *Journal of Petroleum Technology*, *2*(05), 149–154.

[64] **Dean, R.G. and Dalrymple, R.A.** (1991). *Water Wave Mechanics for Engineers and Scientists*, World Scientific Publishing Company.

[65] **Bretschneider, C.** (1968). Significant waves and wave spectrum, *Ocean Industry*.

[66] **Mitsuyasu, H.** (1970). On the growth of the spectrum of wind-generated waves, *Coastal Engineering in Japan*, *13*(1), 1–14.

[67] **Bayindir, C.** (2009). *Implementation of a computational model for random directional seas and underwater acoustics*, University of Delaware.

[68] **Alm, T.**, **Bye, A.**, **Sandvik, K. and Egeland, S.** (1995). The Draugen platform and subsea structures, installation and foundation aspects, *Offshore Technology Conference*, OnePetro.

[69] **URL-1**. `https://draugen.industriminne.no/en/2018/05/14/the-draugen-platform-a-unique-concept/`, date retrieved: 03.05.2022.

[70] **Abolitz, A.L.**, **Anderson, A.R.**, **Birdy, J.N.**, **Boaz, I.**, **Boyd, A.D.**, **Cichanski, W.J.**, **Carino, N.**, **Clarke, J.**, **Davenport, G.F.**, **Dobrowolski, J.A.**, **Duncan, J.**, **Fjeld, S.**, **Gerwick Jr, B.C.**, **Gjørv, O.E.**, **Hognestad, E.**, **lngraham, W.A.**, **Litton, R.W.**, **Mattock, A.H.**, **Runge, K.H.**, **Sharples, B.M.**, **Kokubu, M.**, **Manning, W.F.**, **Smith, C.E.**, **Smith, R.J.**, **Stiansen, S.G.**, **Yee, A.A.**, **Yu, S.Y. and Monnier, T.** (1984). Guide for the Design and Construction of Fixed Offshore Concrete Structures.

[71] **Standartları, T.** (2000). Betonarme Yapıların Tasarım ve Yapım Kuralları (TS500), *Türk Standartları Enstitüsü, Ankara*.

[72] **Noguchi, T. and Nemati, K.** (1995). Relationship between compressive strength and modulus of elasticity of high-strength concrete, *Journal of Structural and Construction Engineering (Transactions of AIJ)*, *60*, 1–10.

[73] **Goodno, B.J. and Gere, J.M.** (2012). *Mechanics of Materials*, Cengage learning.

CURRICULUM VITAE

Barış NAMLI:

EDUCATION:

- **B.Sc.:** 2017, FMV Işık University, Faculty of Engineering and Natural Science, Department of Civil Engineering

PROFESSIONAL EXPERIENCE AND REWARDS:

- 2015 June- 2015 July Engineering Intern at TEMELKON MÜH. İNŞ. SAN. VE TİC. LTD. ŞTİ.
- 2016 August- 2016 September Engineering Intern at BEŞİKTAŞ MUNICIPALITY.

PUBLICATIONS, PRESENTATIONS AND PATENTS ON THE THESIS:

- **Namlı, B., Bayındır, C.** 2021. Vibration Controls of a Pier Using Deep Learning LSTM Network. *The Second International Conference on Applied Mathematics in Engineering*, September 01–03, 2021 Balıkesir, Turkey.
- **Bayındır, C., Namlı, B.** 2021. Efficient sensing of von Kármán vortices using compressive sensing, *Computers Fluids,* 226, 104975.